Controls on the location of compressional deformation on the NW European margin

G. S. KIMBELL[1]*, M. A. STEWART[2], S. GRADMANN[3], P. M. SHANNON[4], T. FUNCK[5], C. HAASE[3], M. S. STOKER[2] & J. R. HOPPER[5]

[1]*British Geological Survey, Keyworth, Nottingham NG12 5GG, UK*

[2]*British Geological Survey, The Lyell Centre, Research Avenue South, Edinburgh EH14 4AP, UK*

[3]*Geological Survey of Norway, Leiv Eirikssons vei 39, 7040 Trondheim, Norway*

[4]*University College Dublin, Belfield, Dublin 4, Ireland*

[5]*Geological Survey of Denmark and Greenland, Øster Voldgade 10, 1350 Copenhagen K, Denmark*

**Correspondence: gsk@bgs.ac.uk*

Abstract: The distribution of Cenozoic compressional structures along the NW European margin has been compared with maps of the thickness of the crystalline crust derived from a compilation of seismic refraction interpretations and gravity modelling, and with the distribution of high-velocity lower crust and/or partially serpentinized upper mantle detected by seismic experiments. Only a subset of the mapped compressional structures coincide with areas susceptible to lithospheric weakening as a result of crustal hyperextension and partial serpentinization of the upper mantle. Notably, partially serpentinized upper mantle is well documented beneath the central part of the southern Rockall Basin, but compressional features are sparse in that area. Where compressional structures have formed but the upper mantle is not serpentinized, simple rheological modelling suggests an alternative weakening mechanism involving ductile lower crust and lithospheric decoupling. The presence of pre-existing weak zones (associated with the properties of the gouge and overpressure in fault zones) and local stress magnitude and orientation are important contributing factors.

The NW European margin records an extensional history spanning from the end of the Caledonian Orogeny to the onset of break-up in the Early Eocene. The Mesozoic part of this evolution progressed from mosaic-like fragmentation of Pangaea in the Permo-Triassic to more systematic east–west extension in the Jurassic, which produced basins elongated in a north–south direction. This was succeeded by NW–SE extension in the Early Cretaceous, and the formation of large basins that cross-cut the older trends (Doré *et al.* 1999). The Cretaceous extension had a major impact on the morphology of the margin, as it involved substantial thinning of the crust beneath a chain of large NE-trending basins (the Lofoten, Vøring, Møre, Faroe–Shetland and Rockall basins: Fig. 1). In the south, similarly high stretching factors beneath the Porcupine Basin include an important contribution from Jurassic extension, whereas the early evolution of the (less stretched) Hatton Basin is poorly understood. From the Eocene onwards, the evolution of parts of the margin was characterized by compressional deformation, with the formation of a series of domes (Fig. 1) (e.g. Doré *et al.* 2008; Ritchie *et al.* 2008; Tuitt *et al.* 2010), although there is also evidence of earlier compression (Doré *et al.* 2008; Tuitt *et al.* 2010; Lundin *et al.* 2013). The aim of this paper is to use results from the NAGTEC project (Hopper *et al.* 2014) to examine the relationship between the siting of the post-break-up compressional structures and the morphology and rheology of the margin established as a consequence of the preceding extensional history.

A key recent hypothesis that addresses this issue has been provided by Lundin & Doré (2011), who argued that the Cenozoic compressional structures were preferentially sited where the lithosphere had previously been highly stretched. They proposed that the lithosphere in these areas was weakened as a result of crustal hyperextension and consequent partial serpentinization of the upper mantle. Hyperextension is a deformation mode affecting

From: Péron-Pinvidic, G., Hopper, J. R., Stoker, M. S., Gaina, C., Doornenbal, J. C., Funck, T. & Árting, U. E. (eds) 2017. *The NE Atlantic Region: A Reappraisal of Crustal Structure, Tectonostratigraphy and Magmatic Evolution*. Geological Society, London, Special Publications, **447**, 249–277.
First published online August 12, 2016, https://doi.org/10.1144/SP447.3

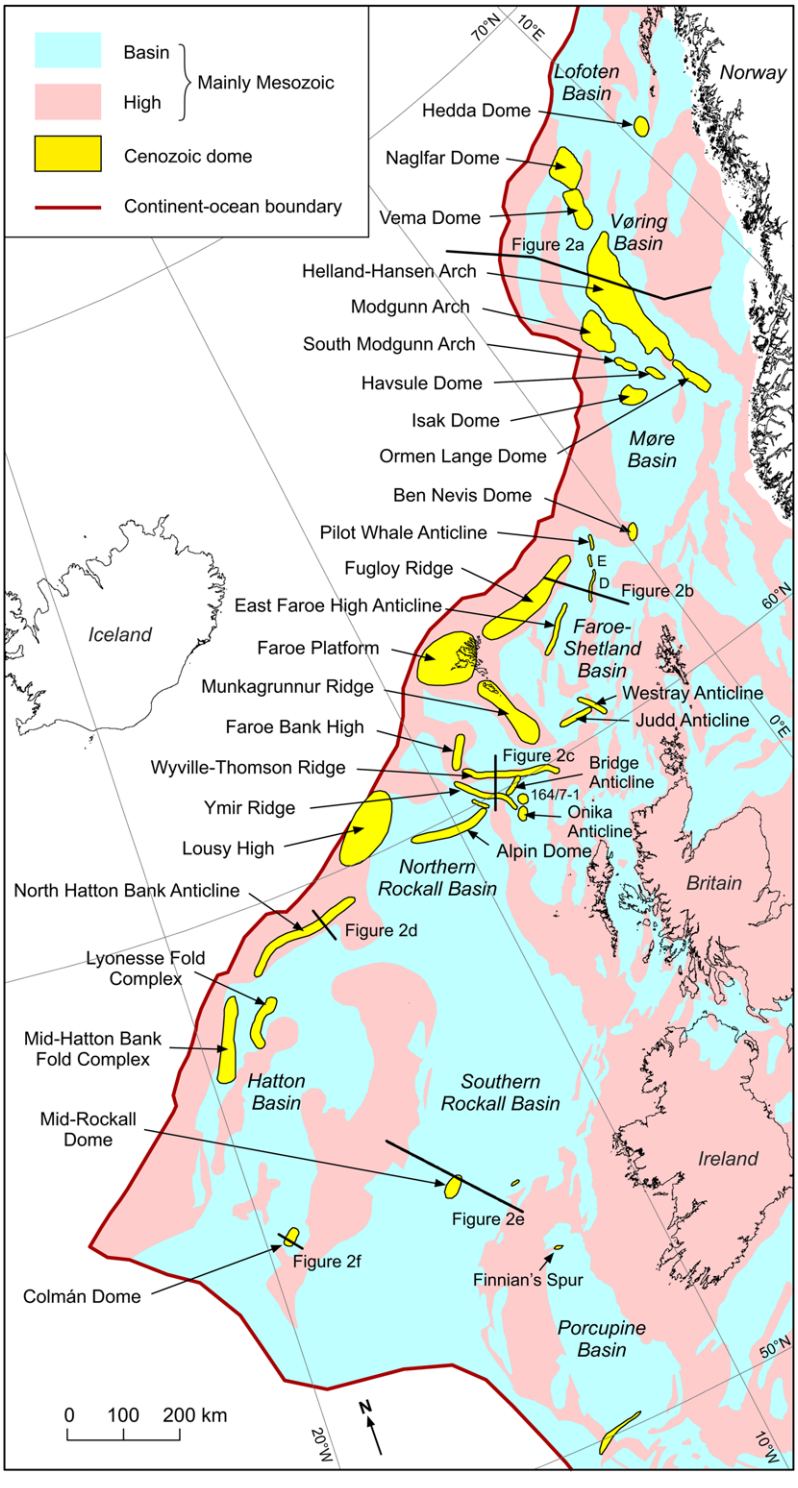

Fig. 1. Location of Cenozoic anticlinal structures on the NW European margin, superimposed on a generalized representation of the structural fabric primarily developed during Mesozoic times.

continental crust that has been thinned to less than 10 km (Unternehr *et al.* 2010; Peron-Pinvidic *et al.* 2013). Serpentinization occurs when water interacts with ultramafic rocks within the stability field of the serpentine minerals (<460°C: Schwartz *et al.* 2013). It is possible for surface water to reach the upper mantle if the entire crust is brittle and is penetrated by faults, but if crustal temperatures are sufficiently high then a ductile lower-crustal layer may form that inhibits such penetration. Although lithospheric extension enhances the geothermal gradient, this applies over a reduced crustal thickness, potentially leading to cooling and embrittlement of the lower crust. The conditions that favour embrittlement are slow extension and low sedimentation rates (a sedimentary layer can have a 'blanketing' effect, increasing temperatures in the underlying crust). Pérez-Gussinyé & Reston (2001) found that stretching factors of between about 3 and 5 were required for embrittlement to occur, depending on the strain rate. The simulations of Rüpke *et al.* (2013) produced similar results when there was no sedimentation, but demonstrated that higher factors were required when the sediment supply was increased.

In the following sections, we: (i) review the compressional structures observed on the NW European margin; (ii) consider their distribution in relation to the characteristics of the underlying crust and the potential for serpentinization of the upper mantle; and (iii) use rheological modelling to explore how the strength of the lithosphere under compression is influenced by its structure, composition (including serpentinization) and thermal state. We use this information to consider how the spatial and temporal variation of multiple factors may have influenced the pattern of deformation observed today.

Cenozoic compressional structures

The following sections briefly review the compressional structures observed on the NW European margin (Fig. 1). These are considered in five broad geographical groupings: Norwegian margin; Faroe–Shetland area; southern Faroe–Shetland to northern Rockall; Hatton margin; and southern Rockall–Hatton–Porcupine.

Norwegian margin

The Helland-Hansen Arch overlies a thick (6–7 km) Cretaceous sedimentary sequence on the eastern side of the Rås Basin, within the Vøring Basin (Figs 1 & 2a) (Blystad *et al.* 1995; Gómez & Vergés 2005). With an axial length of 280 km and maximum amplitude of 1000 m, it is the largest of a number of buried compressional features observed on the Norwegian margin. The structural configuration (Fig. 2a) suggests that at least a component of its Cenozoic growth can be attributed to reverse movements on the Fles Fault Complex (Blystad *et al.* 1995; Brekke 2000). This growth was initiated in the Mid-Eocene–Oligocene, with a second phase occurring in the Miocene (Brekke 2000; Lundin & Doré 2002; Stoker *et al.* 2005*a*). Further growth occurred during the Plio-Pleistocene; Gómez & Vergés (2005) considered this phase to be dominated by differential compaction, and estimated that it may account for up to 70% of the total amplitude of the arch.

Also within the Vøring Basin are the NNE-trending Vema and Naglfar domes (Fig. 1). Both structures underwent initial growth from the Late Eocene to the Early Oligocene, followed by further uplift in the Mid-Miocene continuing to the present day, evidence for which includes active mud diapirs that reach the seafloor (Blystad *et al.* 1995; Gómez & Vergés 2005; Lundin & Doré 2011). East of the Vema Dome, Lundin & Doré (2002) identified the Hedda Dome, with Late Eocene and Early Miocene growth phases. The NW-trending Ormen Lange Dome lies south of the Helland-Hansen Arch and along the same trend (Fig. 1): initial uplift was in the Late Eocene, with another growth phase in the Late Miocene (Blystad *et al.* 1995). West of the Helland-Hansen Arch is the Mogdunn Arch (Fig. 1), and further south are the South Modgunn Arch, the Havsule Dome and the Isak Dome: all of these structures were active in the Miocene (Blystad *et al.* 1995; Lundin & Doré 2002; Doré *et al.* 2008).

Doré *et al.* (2008) identified a set of early 'tectonomagmatic' domes on the Norwegian margin, which are of Late Cretaceous–Paleocene age and related to break-up magmatism. Examples include the Gjallar Ridge (not shown in Fig. 1), and precursors of the Vema and Isak domes.

Faroe–Shetland area

The Fugloy Ridge is a large anticlinal structure that extends ENE from the Faroe Islands. It is asymmetrical, with a steeper SE limb (Fig. 2b), and has a maximum fold amplitude of 3000 m and a bathymetric expression along its length. Boldreel & Andersen (1993, 1995) recognized Paleocene–Eocene and Eocene–Oligocene compressive growth phases, and thinning and onlap in seismic reflection data suggest an enhanced phase of growth in the Mid-Miocene (Fig. 2b), as well as possible further growth during Pliocene to Recent times (Ritchie *et al.* 2003; Johnson *et al.* 2005; Stoker *et al.* 2005*a*). Post-rift thermal subsidence in the flanking Faroe–Shetland Basin has probably enhanced the Fugloy Ridge rather than it being a solely compressional feature (Ritchie *et al.* 2011).

To the east of the Fugloy Ridge lie a number of smaller NE- to NNE-trending compressional

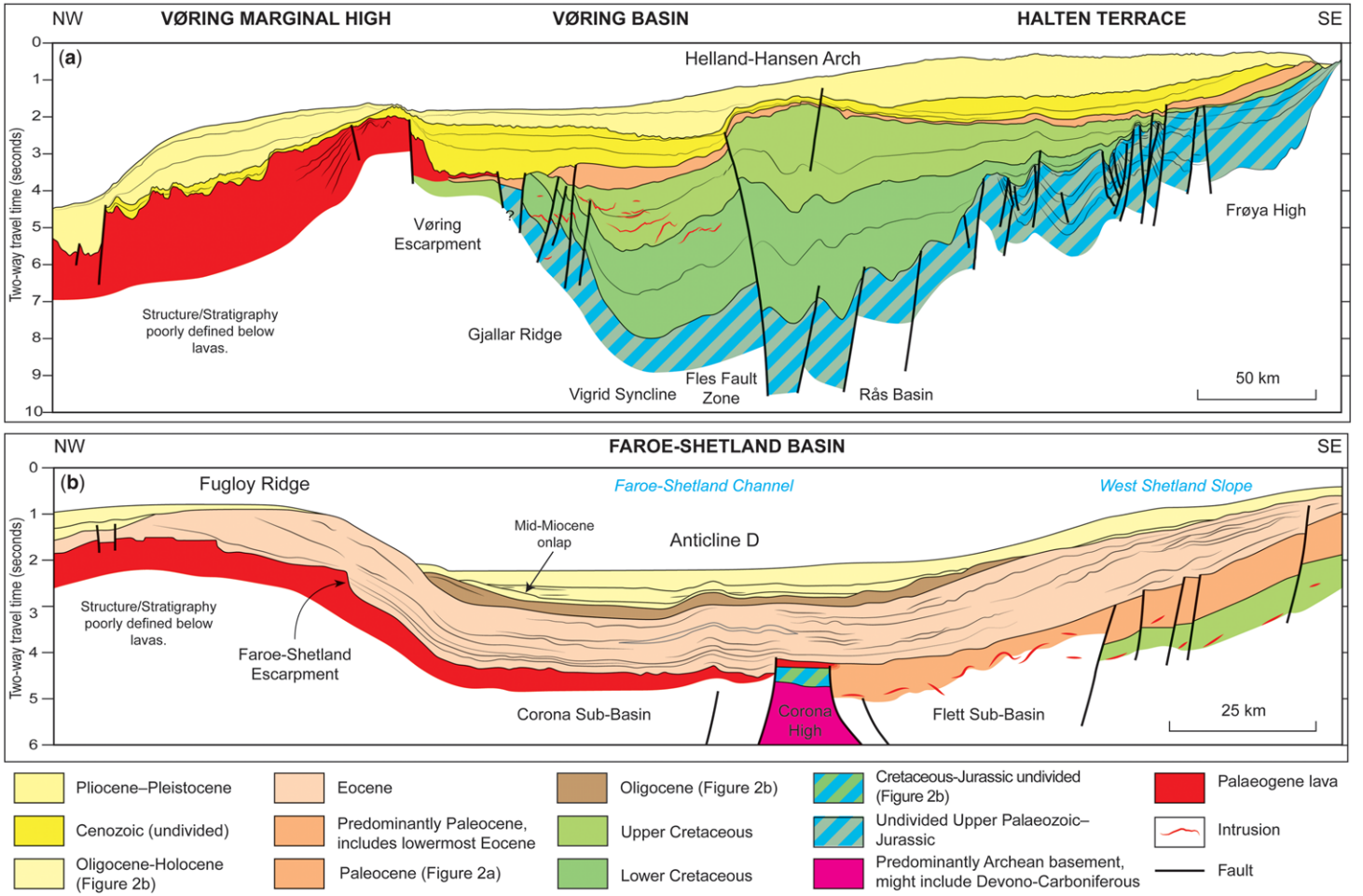

Fig. 2. Geoseismic sections across compressional features, modified from Stoker *et al.* (2014) and references therein. (**a**) Section across the mid-Norwegian margin and the Vøring Basin showing the Helland-Hansen Arch (fig. 7.29c of Stoker *et al.* 2014). (**b**) Section highlighting the Fugloy Ridge and Anticline D compressional structures with Mid-Miocene onlap onto Eocene rocks (fig. 7.21a of Stoker *et al.* 2014).

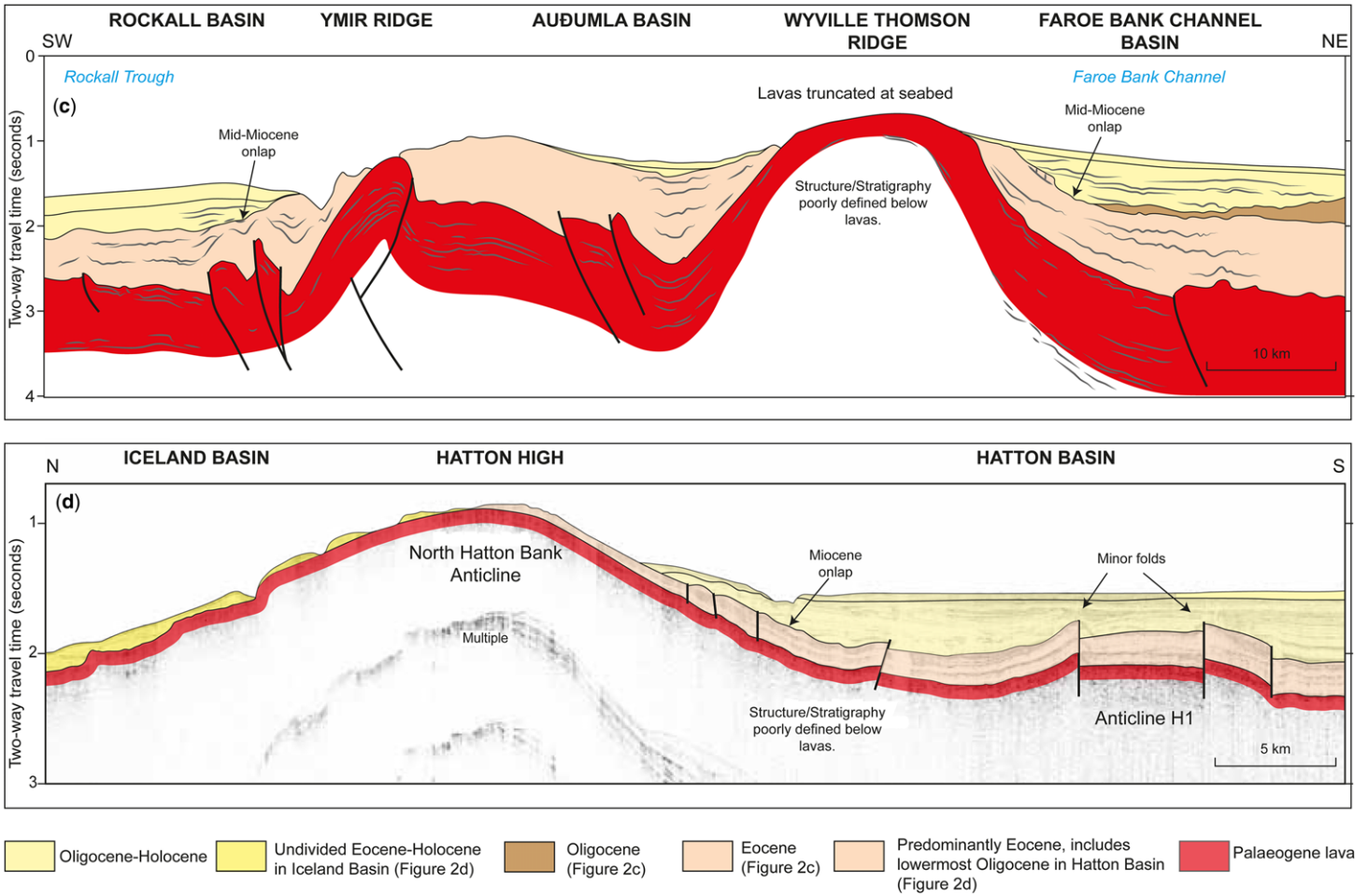

Fig. 2. (**c**) Section showing the Ymir and Wyville Thomson ridges with Mid-Miocene onlap onto the Eocene (fig. 7.21e of Stoker *et al.* 2014). (**d**) Interpreted seismic section (BGS02/02-15) across the Hatton High showing the North Hatton Bank Anticline and Miocene onlap onto the Eocene in the Hatton Basin (fig. 7.25e of Stoker *et al.* 2014).

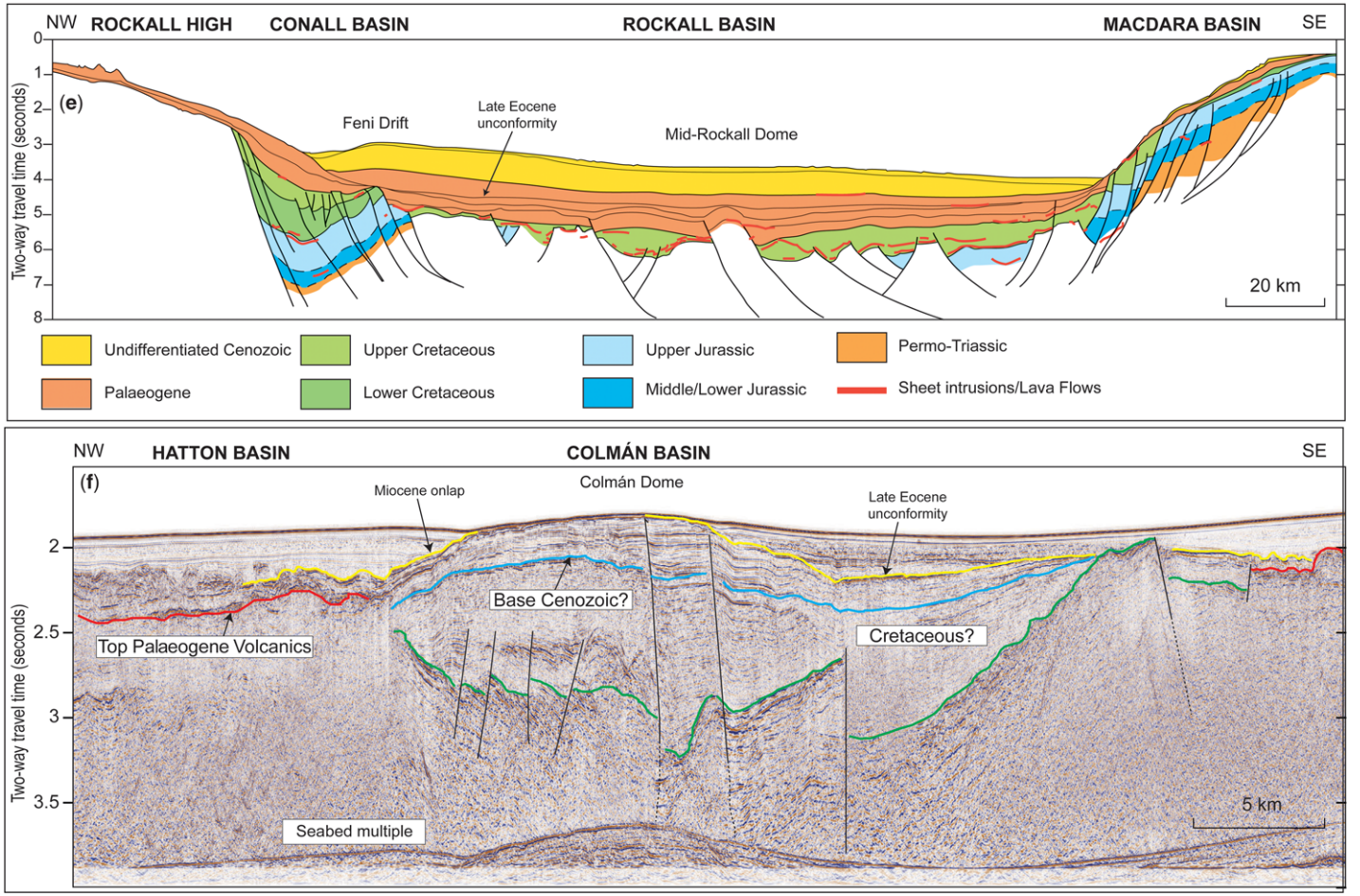

Fig. 2. (**e**) Geoseismic section across the southern Rockall Basin showing the Mid-Rockall Dome and the overlying Late Eocene unconformity (Naylor *et al.* 1999; fig. 7.41e of Stoker *et al.* 2014). (**f**) Seismic section showing the Colmán Dome in the Colmán Basin and the Miocene onlap onto the interpreted Late Eocene unconformity (yellow). Seismic data in (f) was provided courtesy of the Department of Communications, Energy and Natural Resources, Ireland; interpretation based on an unpublished BGS report (D. McInroy pers. comm.).

structures, including the East Faroe High and features termed Anticlines B, D (see Fig. 2b), E and F (the Pilot Whale Anticline) (Davies & Cartwright 2002; Davies *et al.* 2004; Ritchie *et al.* 2003, 2008; Johnson *et al.* 2005). Only selected features are shown in Figure 1: see Ritchie *et al.* (2008) for more detail. These structures were typically initiated in the Mid-Miocene, with further growth in the Early Pliocene; seabed topography suggests that some are still active at the present day (Ritchie *et al.* 2008). Only the younger phase of growth is evident in the case of the Pilot Whale Anticline, which is associated with a number of diapiric structures and mud mounds rising up to 120 m above seabed (Holmes *et al.* 2003). The Ben Nevis Dome is a buried anticline, overlain by basalts, which lies 12 km SE of the large, igneous, Brendan Dome (Fig. 1). Hodges *et al.* (1999) proposed that it formed as a result of the latest Paleocene uplift of a Jurassic fault block driven by igneous intrusion from the Brendan Dome and inversion of the Cretaceous fill of an adjacent half-graben. Rohrman (2007) suggested its formation at around 65–60 Ma (i.e. Paleocene), coincident with the intrusion of an underlying igneous pluton.

In the SW Faroe–Shetland Basin lie the Judd and Westray anticlines, which trend to the west and NW respectively (Fig. 1) (Smallwood & Kirk 2005; Ritchie *et al.* 2008; Stoker *et al.* 2013). The Judd Anticline is 33 km long, and had growth phases in the Early and Mid-Eocene and probably in the Oligocene. The Westray Anticline is 45 km long and intersects the eastern part of the Judd Anticline (Fig. 1). Growth occurred during the Eocene, Late Eocene–Oligocene and the Miocene, with further growth possible up to the present day (Ritchie *et al.* 2008).

To the south of the Faroe Platform, the Munkagrunnur Ridge is a NNW-trending 135 km-long anticline with seabed expression (Boldreel & Andersen 1993; Johnson *et al.* 2005; Ritchie *et al.* 2008, 2011). Boldreel & Andersen (1993) suggested that the ridge is part of a set of ramp-anticlines, along with the Ymir and Wyville Thomson ridges, which formed during the Late Paleocene–Eocene above a northwards-dipping crustal fault in response to seafloor spreading. The Faroe Bank Channel, which separates the Wyville Thomson and Munkagrunnur ridges, may be a synclinal feature formed in response to the growth of those anticlines, especially in the late Palaeogene–early Neogene, and is an important part of the North Atlantic deep-water circulation system (Stoker *et al.* 2005*a*).

Southern Faroe–Shetland Basin to the northern Rockall Basin

The Wyville Thomson Ridge is a 200 km-long WNW-trending basalt anticline with a maximum fold amplitude of 4000 m, a width of around 20 km and clear bathymetric expression (Boldreel & Andersen 1993; Johnson *et al.* 2005; Stoker *et al.* 2005*a*, *b*; Ritchie *et al.* 2011). A well-imaged succession on the NE side of the ridge shows thinning of Paleocene lavas and Early and Mid-Eocene sediments towards its axis, indicative of growth periods (Fig. 2c) (Boldreel & Andersen 1998; Johnson *et al.* 2005). Further thinning and growth is recognized in the early Oligocene (Johnson *et al.* 2005; Tuitt *et al.* 2010), and a series of unconformities indicates a major growth period in the middle Miocene (Fig. 2c) (Boldreel & Andersen 1998; Johnson *et al.* 2005; Stoker *et al.* 2005*a*, *b*).

The Ymir Ridge is a NW-trending asymmetrical anticline up to 100 km in length, with a maximum amplitude of 3500 m and bathymetric expression along most of its length. It is characterized by the presence of reverse faults, especially apparent in the Central Ymir Ridge identified by Ziska & Varming (2008), with growth folding observed in the Eocene–Oligocene succession of the SW flank (Fig. 2c) (Boldreel & Andersen 1993; Johnson *et al.* 2005; Ritchie *et al.* 2008). A number of unconformities also indicate middle Miocene growth.

The Bridge Anticline trends NE between the Wyville Thomson Ridge and the Ymir Ridge (Fig. 1), and has an amplitude of up to 1200 m: it was interpreted by Tuitt *et al.* (2010) as originating in the Mid-Eocene. The Onika Anticline trends NNE with an amplitude of 800 m and is inferred to have grown during the Late Eocene (Tuitt *et al.* 2010). The Alpin Dome is an eastwards-trending anticline up to 150 km in length; onlap and thinning suggest growth during the Late Eocene and Oligocene (Tuitt *et al.* 2010), with middle Miocene compression also suggested by Stoker *et al.* (2005*a*) and Ritchie *et al.* (2008). A domal structure drilled by well 164/7-1 is inferred to have an igneous origin (Archer *et al.* 2005).

The NE-trending Lousy High (Fig. 1) marks the western edge of the northern Rockall Basin and forms an elongated bathymetric feature 125 km long (Tuitt *et al.* 2010; Ritchie *et al.* 2013). A latest Eocene age is suggested by Tuitt *et al.* (2010).

Hatton margin

The North Hatton Bank Anticline (Figs 1 & 2d) (Hitchen 2004; Johnson *et al.* 2005) can be traced for 220 km, and has a wavelength of 40 km and a maximum amplitude of 1900 m (Johnson *et al.* 2005; Tuitt *et al.* 2010). Tuitt *et al.* (2010) recognized three discrete examples of onlap onto the structure within the Eocene in seismic reflection data, with Late Eocene reverse faulting and onlap also observed by Johnson *et al.* (2005), indicative of a major growth phase (Fig. 2d). The NE-trending

Lyonesse Fold Complex has a length of 50 km, a maximum amplitude of 100 m and an age of formation constrained by folding of the Late Eocene unconformity (Johnson *et al.* 2005). Folding in the Mid-Hatton Bank Fold Complex post-dates the Albian rocks recovered from shallow boreholes (Hitchen 2004) and pre-dates the overlying flat-lying Cenozoic strata, which include Early Eocene and Late Eocene unconformities (Johnson *et al.* 2005, fig. 9).

Southern Rockall, Hatton and Porcupine basins

The southern Rockall Basin contains few obvious Cenozoic compressional structures, with the clearest of these lying beneath the central part of the basin (Figs 1 & 2e) (Naylor *et al.* 1999; McDonnell & Shannon 2001; Morewood *et al.* 2004). Resolution is limited by a lack of seismic coverage, but the structure (herein termed the Mid-Rockall Dome) appears to be a NE-trending broad dome underlain by a set of eastwards-dipping late Cretaceous–earliest Cenozoic faults. Growth faulting and onlap of the Paleocene–earliest Eocene strata suggest structural (probably fault) control on its location and, together with truncation by the regional Late Eocene unconformity, a Late Eocene age for its formation.

Another inversion structure (herein termed the Colmán Dome) is apparent in the Colmán Basin on the SE flank of the Hatton Basin, where there is pronounced doming of the Late Eocene unconformity and an expression at the seabed (Fig. 2f). This suggests an Oligocene or younger age of formation. The seismic section shown in Figure 2 was acquired in an area where the Palaeogene volcanic rocks are thin or absent, providing a 'window' through which the underlying structure can be viewed. A deeper sequence is imaged that is likely to be mainly Cretaceous in age (possibly underlain by Jurassic rocks), although the age of individual reflectors is poorly constrained. The structures revealed strongly suggest that the dome was formed by inversion of the underlying basin.

A compressional structure is observed in the south of the Porcupine Basin (southernmost feature in Fig. 1). It is approximately 100 km in length and was described by Masson & Parson (1983) as changing from a complex faulted anticline in the west to a simple monocline in the east. Those authors inferred that it developed in late Eocene time along a pre-existing geological lineament. It has an east–west orientation, and is coincident along part of its northern margin with a large fault (Naylor *et al.* 2002).

Just south of Finnian's Spur in the Porcupine Basin (Fig. 1) is a possible inversion structure identified by Naylor *et al.* (2002) and associated with the Finnian's Spur basement ridge between the Porcupine and North Porcupine basins. The feature is apparent within the Upper Cretaceous section above the southern bounding fault of the spur, and is probably Palaeogene in age.

Geophysical evidence for hyperextension and mantle serpentinization

Figure 3 is a map of the thickness of the crystalline crust along the NW European margin, based on the compilation of seismic refraction data of Funck *et al.* (2014, this volume, in press). Figure 4 shows the crustal thickness derived by gravity modelling (Funck *et al.* 2014; Haase *et al.*, this volume, in review). The display is designed to highlight areas where hyperextension has occurred. The two maps are not fully independent because constraints based on the seismic refraction data were applied during the gravity inversion, and the refraction interpolation used a kriging technique guided by the gravity anomaly. The gravity inversion, however, includes a number of additional constraints, such as sediment thickness based on seismic reflection data and wells (see Hopper *et al.*, this volume, in prep). Stretching factors (original thickness divided by the stretched thickness) are also indicated on these figures, but these are based on a pre-rift crustal thickness that is difficult to define accurately. A reference value of 30 km is estimated around Britain and Ireland on the basis of observed crustal thicknesses in areas where topography lies close to sea level and Mesozoic basins are absent (e.g. Jacob *et al.* 1985; Lowe & Jacob 1989). In the Norwegian sector, larger crustal thicknesses have been detected in the coastal region (e.g. 35–40 km on profile 2 of Kvarven *et al.* 2014) and used as a reference in the construction of gravity models (e.g. 35 km used by Ebbing 2007). Skogseid *et al.* (2000) discussed the issues associated with defining pre-rift thickness on this margin and presented a methodology for inferring it with respect to Late Jurassic–Early Cretaceous rifting. Their models suggest values of about 30 km for the Møre and Vøring basins, and so provide some justification for extending the UK/Ireland thickness assumption into this area.

The degree of stretching shown in Figures 3 and 4 will be underestimated where the mapped crystalline crust includes igneous additions or partially serpentinized upper mantle. Igneous additions are likely to occur adjacent to the continental margin and these or serpentinized upper mantle may be present further inboard on the Norwegian margin, but the stretching is less likely to be underestimated in the Rockall Basin area (see the further discussion below).

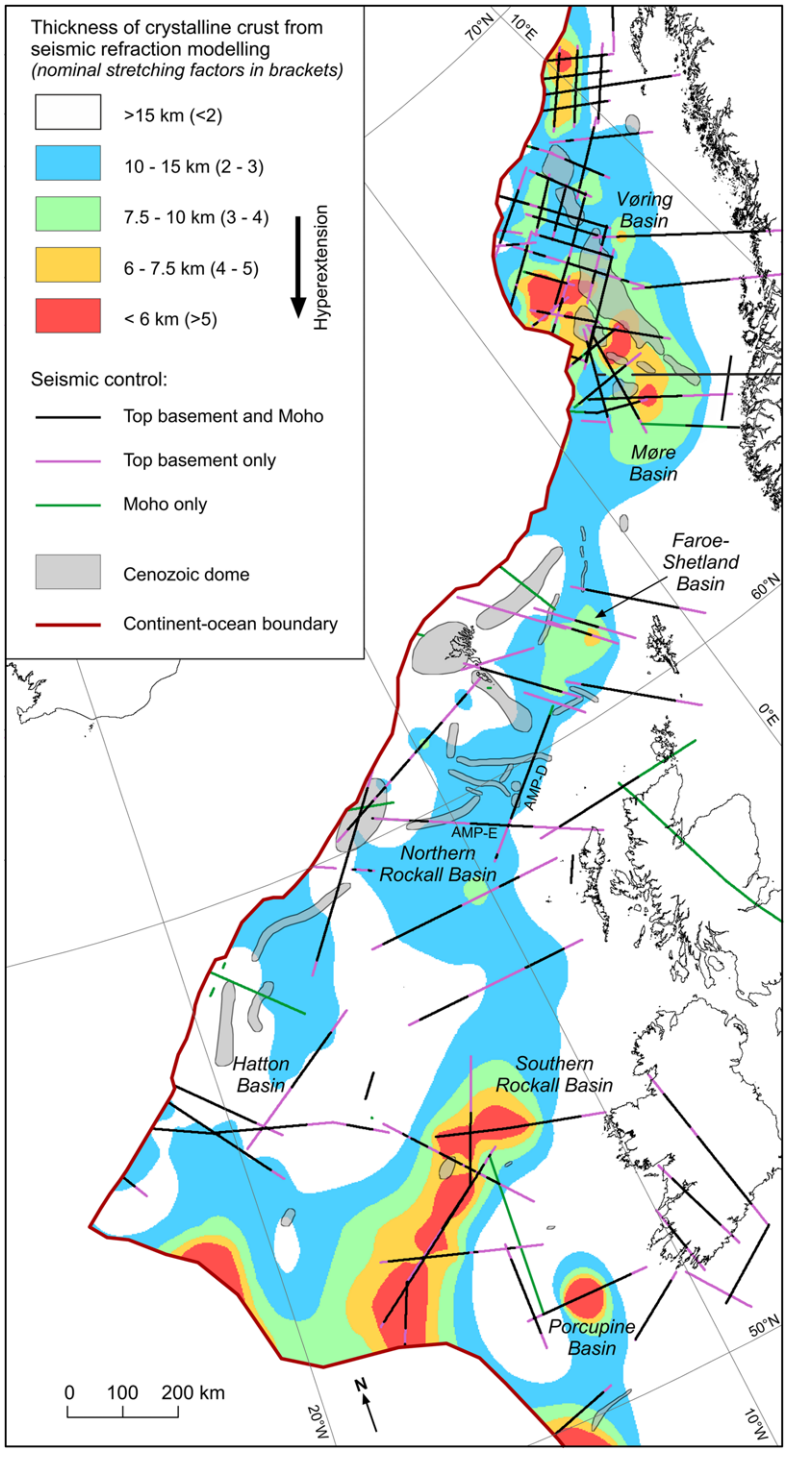

Fig. 3. Thickness of crystalline crust on the NW European margin based on the seismic refraction compilation of Funck *et al.* (2014, this volume, in press). Nominal stretching factors are based on an initial crustal thickness of 30 km (see the text).

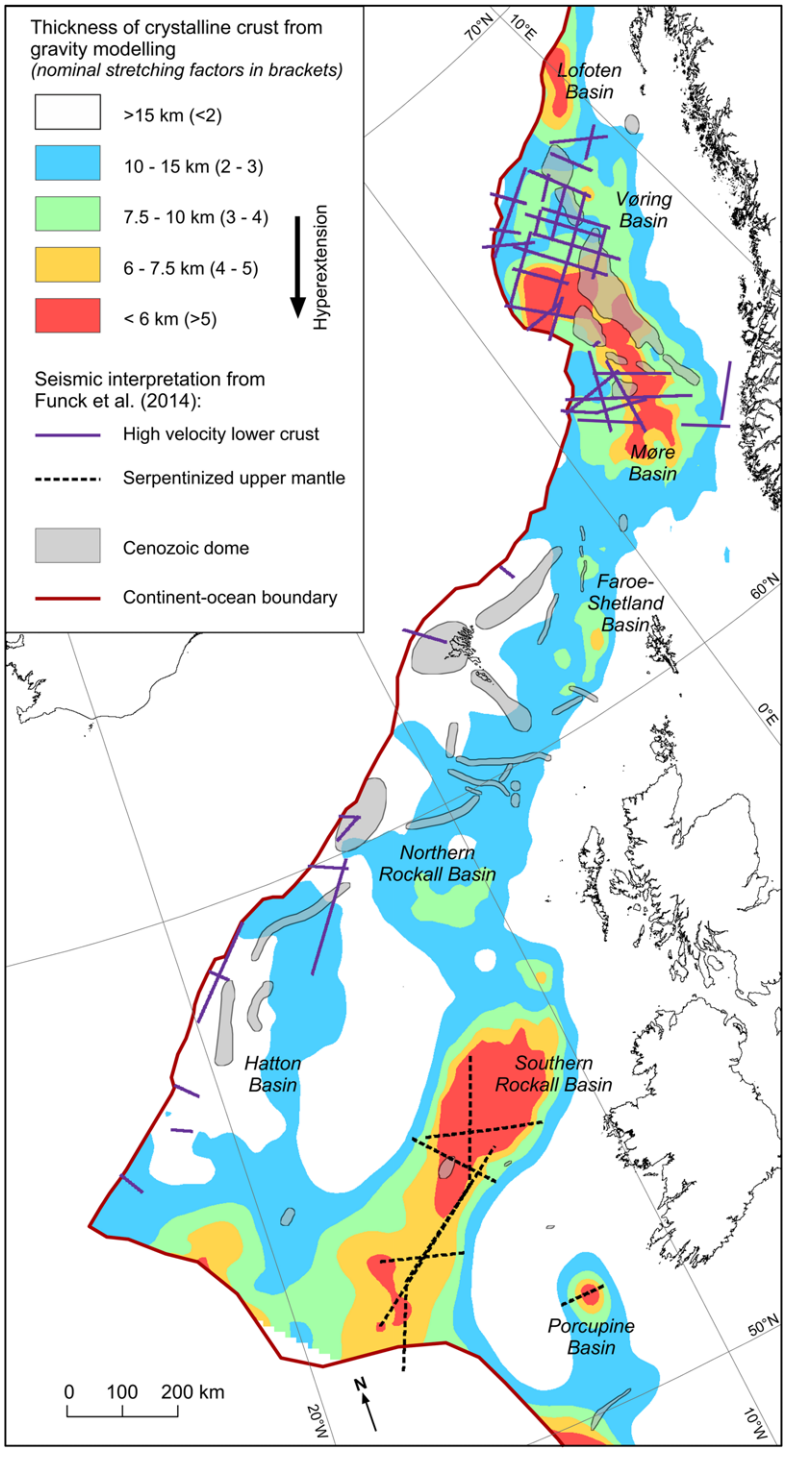

Fig. 4. Thickness of crystalline crust on the NW European margin based on the gravity inversion described by Funck *et al.* (2014) and Haase *et al.* (this volume, in review). Note that alternative interpretations of the high velocity lower crust in the northern part of the area include serpentinized upper mantle (see the text).

The maps indicate several areas where the crust is thin enough to be potentially conducive to serpentinization of the upper mantle (crystalline crustal thickness <10 km: green, orange and red zones in Figs 3 & 4). These cover much of the Norwegian margin (the Lofoten Basin, southern Vøring Basin and the Møre Basin), the southern Rockall Basin and the Porcupine Basin. They are less extensive beneath the Faroe–Shetland Basin and absent beneath most of the northern Rockall Basin. There are differences in detail (e.g. the model derived from gravity inversion extends the hyperextended zone in the southern Rockall Basin further to the north), but these broad observations are compatible with both maps.

Seismic refraction surveys can provide evidence of serpentinization through its influence on the seismic properties of the upper-mantle rocks. There is a linear relationship between the degree of serpentinization and the P-wave velocity, with a reduction from about 8.0 km s^{-1} in unserpentinized peridotite to 4.5–5.0 km s^{-1} when fully serpentinized to lizardite/chrysotile (Christensen 2004). This overlaps with the seismic velocity range of lower-crustal and gabbroic rocks, leading to a potential ambiguity in interpretation. The relatively high Poisson's ratio of the serpentinized rocks (Christensen 2004) can help to reduce the ambiguity, as can the presence of a gradational rather than sharp transition to normal mantle velocities at depth (Minshull 2009). There are, nonetheless, areas where the distinction between high-velocity lower crust (HVLC) and serpentinized upper mantle remains equivocal, as discussed in the following subsections. Figure 4 shows where units falling within these two categories have previously been identified along the NW European margin, based on the categorization of Funck *et al.* (2014).

Norwegian margin

High-velocity lower crust (HVLC) has been mapped over large parts of the Norwegian margin, and its origin has been much debated. Alternative explanations fall into three categories: basic igneous rocks (underplated material); high-grade metamorphic rocks; and partially serpentinized upper mantle (Mjelde *et al.* 2002, 2009*b*).

In the north, the Lofoten margin appears to be devoid of HVLC, despite the fact that extensive volcanic flows and seaward-dipping reflectors (SDRs) occur and have been linked to underplating in other areas. In the central segment of the Vøring margin, HVLC with a thickness of up to 8 km has been mapped by many seismic refraction and reflection experiments, and additionally constrained using gravity data and isostatic modelling (e.g. Gernigon *et al.* 2003, 2004; Ebbing *et al.* 2006; Mjelde *et al.* 2009*a*; Reynisson *et al.* 2010). HVLC has also been detected on the Møre margin, south of the Jan Mayen Lineament, and in that area an additional zone has been detected in the east, close to the shelf edge (Kvarven *et al.* 2014).

The HVLC of the central and northern Vøring margin exhibits velocities of 7.2–7.4 km s^{-1} (locally up to 7.6 km s^{-1}) and ratios of compressional to shear wave velocity (V_p/V_s) of 1.8–1.9, which do not, in themselves, differentiate between the alternative explanations for its origin. Gernigon *et al.* (2003, 2004) showed that there is not a simple correlation between observable crustal extension and the distribution and thickness of high-velocity lower-crustal bodies. On the contrary, on the Vøring margin, such bodies tend to correlate with structural highs (and, thus, with thicker overlying crystalline crust). Furthermore, correlation with the regional fault system suggests that the HVLC was already in place before break-up. Gernigon *et al.* (2003, 2004) interpreted the HVLC to comprise high-pressure metamorphic rocks (granulite/eclogite facies), as observed in the Caledonian nappes onshore. Magmatic underplating associated with the influence of a thermal anomaly prior to ocean opening between Norway and Greenland has been suggested by Skogseid *et al.* (1992) and Mjelde *et al.* (1997). A lower crust containing mafic intrusions emplaced close to the time of break-up is favoured by Mjelde *et al.* (2009*a*). Reynisson *et al.* (2010), Lundin & Doré (2011) and Rüpke *et al.* (2013) advocate partially serpentinized upper mantle. The HVLC of the southern Vøring margin (adjacent to the Jan Mayen Fracture Zone) exhibits P-wave velocities of up to 8.4 km s^{-1}, which suggest an eclogitic rather than peridotitic nature (Mjelde *et al.* 2009*a*).

The HVLC beneath the outer part of the Møre margin has been mapped in a refraction seismic study by Mjelde *et al.* (2009*b*), and corroborated by reflection seismic and gravity data (Nirrengarten *et al.* 2014). Here, the overlying crust is less than 10 km thick, making a serpentinized upper-mantle origin possible, although extensive volcanic sills and SDRs suggest significant magmatic activity. Any of the three main origins for high-velocity lower crust is thus plausible here. The inner zone of the HVLC on the Møre margin is located near the coast along the shelf edge and correlates well with a regional gravity high (Olafsson *et al.* 1992; Kvarven *et al.* 2014; Nirrengarten *et al.* 2014). The HVLC extends beneath crystalline crust that is more than 15 km thick, suggesting that fluid penetration and serpentinization of the uppermost mantle is unlikely. Eclogitic crust from the Western Gneiss Region is widespread on the adjacent mainland, making an eclogitic origin for the HVLC more likely.

HVLC adjacent to the ocean margin

The hypotheses for the HVLC on the Norwegian margin are not mutually exclusive, and proponents of partially serpentinized upper mantle beneath parts of the margin have also embraced a break-up-related magmatic origin where the HVLC lies adjacent to the continent–ocean boundary (Reynisson *et al.* 2010; Lundin & Doré 2011; Rüpke *et al.* 2013). A magmatic origin has also been the preferred interpretation for the HVLC detected adjacent to the ocean margin in a series of seismic refraction experiments further south. Near the Faroe Islands and beneath the northern part of Hatton Bank, the iSIMM experiments revealed a 40–50 km-wide zone of HVLC that was interpreted to be due to the intrusion of basic igneous sills at the time of break-up (White *et al.* 2008; Roberts *et al.* 2009; White & Smith 2009). Funck *et al.* (2008) identified an extension of the HVLC beneath the northern part of the Hatton Basin below crystalline crust about 10 km thick, and interpreted this to be due to magmatic additions to the crust rather than partial serpentinization of the upper mantle. Further south, a zone of HVLC has been detected beneath the Hatton continental margin, overlain by crust in which the lower layer has been completely attenuated (Vogt *et al.* 1998; Shannon *et al.* 1999). The HVLC can be traced southwards beneath the SDRs on Edoras Bank (Barton & White 1997).

Faroe–Shetland Basin

The crustal thickness beneath the Faroe–Shetland Basin is poorly resolved by seismic refraction experiments and there are some contradictory results (Petersen & Funck, this volume, in press). A minimum thickness of 7–8 km has been identified (Makris *et al.* 2009), although gravity modelling suggests that values of 10–12 km are more widespread (Haase *et al.*, this volume, in review). Raum *et al.* (2005) and Makris *et al.* (2009) report upper-mantle velocities of about 8.0 km s^{-1} beneath the basin.

Northern Rockall Basin

A seismic refraction profile across the northern part of the Rockall Basin (AMP-E: Fig. 3) (Klingelhöfer *et al.* 2005) detected crystalline crust with a minimum thickness of 10–12 km. The Moho beneath this profile was primarily identified using PmP reflections, so it is not possible to infer the velocity structure of the underlying mantle. However, an orthogonal line extending from the northern Rockall Basin into the southern Faroe–Shetland Basin (AMP-D: Fig. 3) (Klingelhöfer *et al.* 2005) did detect diving rays into the mantle (Pn), beneath 11–13 km-thick crust in an area affected by compressional deformation, and these indicated an upper-mantle velocity of 8.0–8.2 km s^{-1}. An early (unreversed) refraction experiment also detected clear Pn arrivals indicative of an upper-mantle velocity of 8.2 $\pm$ 0.17 km s^{-1} beneath the northern Rockall Basin (Bott *et al.* 1979). Thus, there is no direct evidence at present for serpentinization beneath this basin.

Southern Rockall Basin

Seismic refraction data indicate that the crystalline crust beneath the southern part of the Rockall Basin is typically 5–7 km thick (Shannon *et al.* 1999; Morewood *et al.* 2005). This is underlain by a 3–10 km-thick zone with P-wave velocities of 7.5–7.8 km s^{-1}, which was interpreted as a partially serpentinized upper mantle by O'Reilly *et al.* (1996). The geometry of the zone, its velocity range and the V_p/V_s ratios (1.80–1.83) were considered to favour this interpretation over one involving igneous underplating. The velocities indicate a degree of serpentinization of 10–15%. Further support for a serpentinization model comes from the subsidence discrepancy along the axis of the basin (O'Reilly *et al.* 1996). The observed subsidence is consistently 400–600 m less than modelled subsidence over the zone of interpreted serpentinization, while there is no discrepancy to the north and south, making it less likely that the abnormal subsidence is due to a thermal anomaly (Joppen & White 1990).

Hauser *et al.* (1995) and O'Reilly *et al.* (1996) observed that the slow stretching rates necessary to explain hyperextension without magmatism were most easily explained by a differential stretching model in which the upper and middle crust were more extended than the lower crust and upper mantle. This interpretation was supported by a comparison between the three-layer velocity model for adjacent, unstretched crust (Jacob *et al.* 1985; Lowe & Jacob 1989) and the velocity structure observed beneath the central part of the basin.

Porcupine Basin

A seismic refraction experiment across the Porcupine Basin resolved severely and asymmetrically stretched (<2 km-thick) continental crust beneath thick sedimentary cover in the centre of the basin (O'Reilly *et al.* 2006). The velocity of the uppermost part of the mantle beneath the thinned crust lies in the range 7.2–7.5 km s^{-1}, increasing to around 8 km s^{-1} over a depth of about 20 km. O'Reilly *et al.* (2006) interpreted this zone to be serpentinized upper mantle, and discounted the

alternative explanation of magmatic underplating on the basis of the absence of a characteristic double PmP reflection (typically seen from the top and bottom of such bodies) and the lack of evidence for extensive magmatic activity in this part of the basin at the time of stretching. The velocities encountered suggest a degree of serpentinization of up to 25%.

Rheological modelling

Construction of yield strength envelopes

The yield-strength envelope is used to predict the way in which lithospheric strength varies with depth and to analyse how this is influenced by factors such as the thickness and composition of the crust, the presence of fluids, the temperature regime, and the strain rate. We have constructed a series of such envelopes representing the range of conditions encountered along the NW European margin in order to see whether these can help to explain the distribution of compressional structures. This method is commonly used to explore lithospheric strength profiles in various geological settings (e.g. Jackson 2002; Burov & Watts 2006; Cloetingh *et al.* 2008; Burov 2011 and references therein), but has only rarely been applied to a lithosphere that includes partially serpentinized upper mantle (Escartín *et al.* 1997*a*; Pérez-Gussinyé & Reston 2001).

The envelopes were constructed by combining predictions about the brittle and ductile behaviour of lithospheric rocks. At shallow depth, brittle deformation dominates and is controlled by friction effects that are mainly dependent on the depth of burial. As temperature increases with depth, a point is reached beyond which ductile deformation occurs at lower stresses than brittle failure. In oceanic lithosphere, the result is typically a single strong layer with a thickness that increases with age. In continental lithosphere, more than one strong layer may occur as a result of changes in lithology. For example, the strong upper crust may be decoupled from a strong upper mantle by a ductile lower crust (the 'jelly sandwich' model) (Hopper & Buck 1998).

Yield-strength envelopes are presented in Figure 5 for simple models representing 'normal' (30 km) thickness continental crust (Fig. 5a, b), highly extended crust as encountered, for example, in the northern Rockall Basin (Fig. 5c, d: 5 km of sediments over 12 km of crystalline crust) and hyperextended crust as in the southern Rockall Basin (Fig. 5e, f: 6 km of sediments over 6 km of crystalline crust). The envelopes shown in Figure 5g, j are more representative of the Norwegian margin, where hyperextended crust is overlain by a much thicker sedimentary layer. In Figure 5g, h, 12 km of sediments overlie a crust with a thickness of 8 km. The Moho depth is the same in Figure 5i, j, but in that case a 10 km sedimentary layer overlies 5 km of crystalline crust underlain by 5 km of high-velocity lower crust (HVLC).

In each example, the compressive-strength envelope was calculated on the basis of both 'cool' and 'warm' geotherms (panels on the left- and right-hand side of Fig. 5, respectively). Table 1 lists the thermal parameters assumed in calculating these. The boundary conditions for an initial steady-state model were a surface temperature of 0°C, and alternative mantle heat flows of 25 and 40 mW m^{-2}, respectively. In the stretched models, the small residual thermal effect of the original Mesozoic rifting event was simulated in a simple fashion by the addition of a thermal anomaly calculated using the method and parameters of McKenzie (1978), assuming instantaneous Early Cretaceous (140 Ma) rifting.

The geotherms do not incorporate the details of factors such as the distribution of heat-producing elements in the crust (and the way this is influenced by stretching), and the influence of porosity and lithology on the thermal conductivity of the sedimentary layer. They are not intended to provide a specific simulation, but, rather, a range of temperature profiles that allows an assessment of the sensitivity of lithospheric rheology to thermal conditions. Even with these limitations, it might be hoped that a comparison of measured heat flows with predicted values (indicated towards the bottom of each panel in Fig. 5) would provide a general indication of the present-day strength envelopes across the region. In practice, problems with the availability and accuracy of heat-flow measurements severely limit the confidence with which that calibration can be made. Measured heat flows in basinal settings can be distorted by factors such as recent sedimentation and erosion, refraction into basement highs, and hydrothermal convection. In very broad terms, the representative models for the southern part of the area (Fig. 5a–f) appear to bracket the typical heat flows observed there, whereas the more extensive heat-flow data available for the Norwegian margin and, in particular, the Vøring Basin (Sundvor *et al.* 2000; Ritter *et al.* 2004) suggest a thermal state closer to the warm models than the cool models.

The strength in the brittle parts of the yield-strength envelope was calculated with reference to the Anderson theory of faulting (Anderson 1951; Turcotte & Schubert 2002):

$$\Delta\sigma = \frac{2f_s(\rho gz - \rho_w gz)}{\sqrt{(1+f_s^2)} - f_s}$$

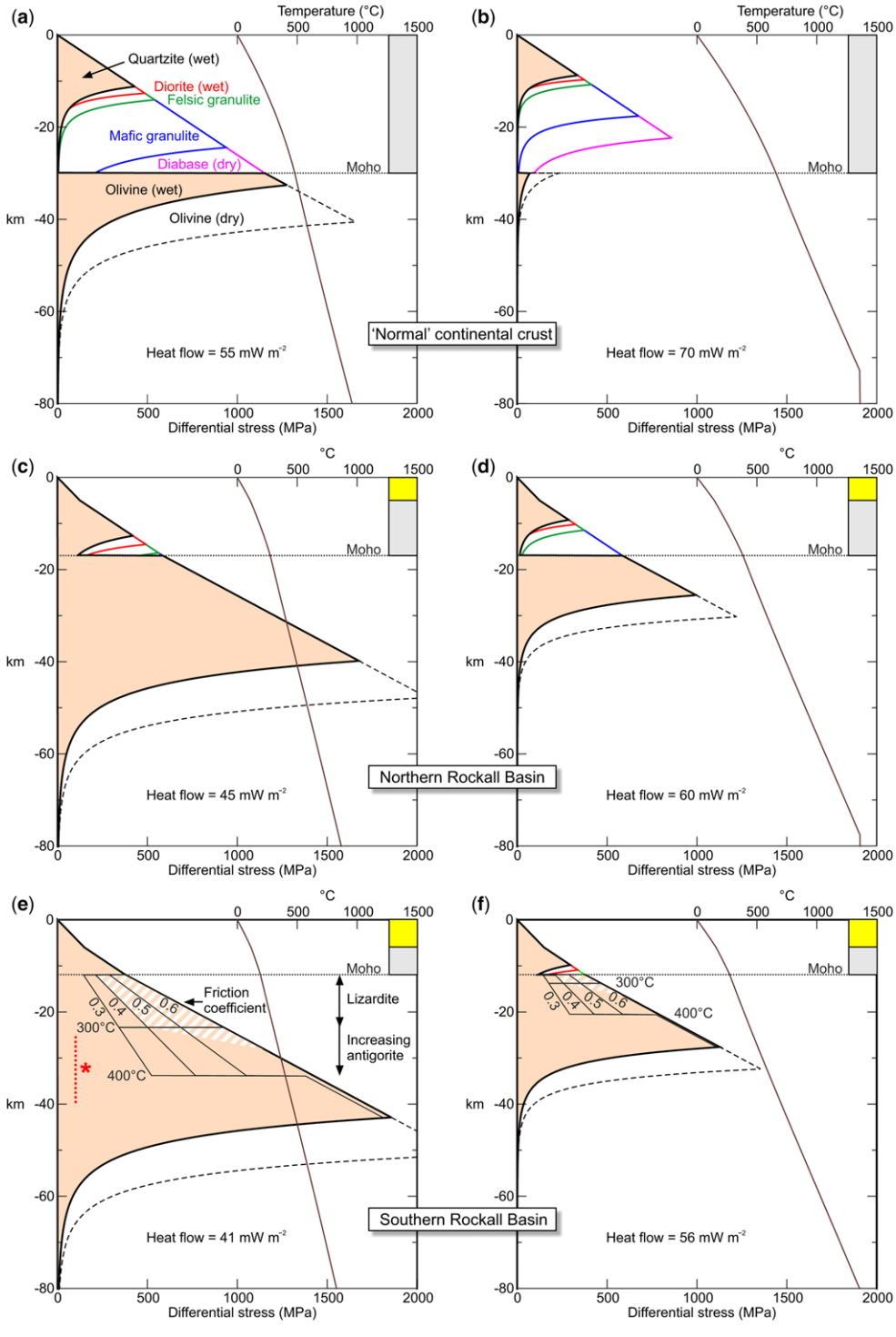

Fig. 5. Theoretical yield-strength envelopes for different simple crustal configurations: (**a**) and (**b**) 30 km-thick crystalline crust; (**c**) and (**d**) 5 km of sediments over 12 km of crystalline crust; (**e**) and (**f**) 6 km of sediments over 6 km of crystalline crust.

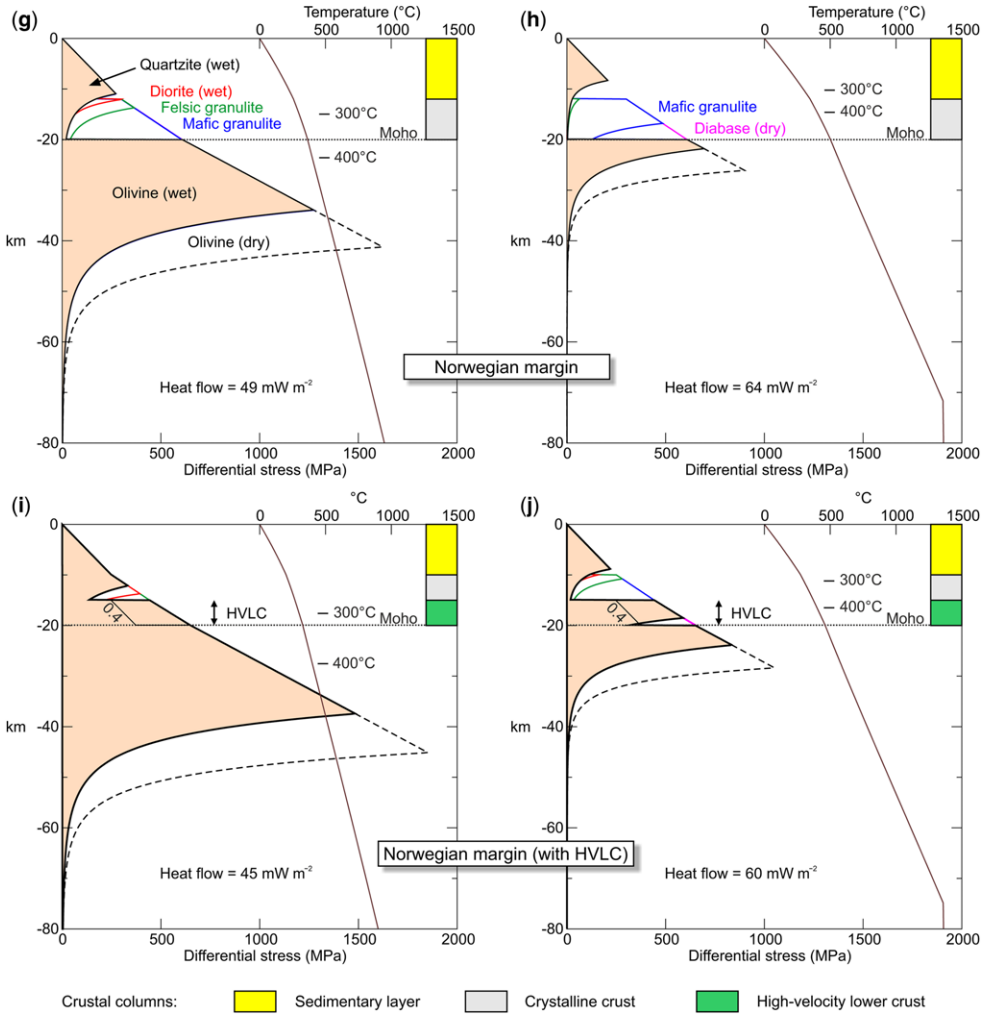

Fig. 5. (**g**) and (**h**) 12 km of sediments over 8 km of crystalline crust; (**i**) and (**j**) 10 km of sediments over 10 km of crystalline crust, of which 5 km is HVLC. The envelopes are for failure under compression (brittle failure occurs at lower stresses under extension). Depths are relative to ground surface/seabed. Each configuration is modelled with alternative 'cool' (a, c, e, g & i) and 'warm' (b, d, f, h & j) conditions (geotherms are shown on the right-hand side of the figures). The additional lines on the example shown in (e) and (f) illustrate the effect of different coefficients of friction within a zone of partially serpentinized upper mantle, and the hachured zone illustrates how the yield-strength envelope might be modified within this zone (see the text). The 0.4 friction coefficient is also shown in the zone of high-velocity lower crust in (i) and (j). The red dashed line marked with an asterix in (e) indicates the depth range within which there is potential for weakening associated with the ductile deformation of antigorite (Hilairet *et al.* 2007).

where $\Delta\sigma$ is the maximum horizontal deviatoric stress that can be withstood under compression, f_s is the coefficient of internal friction (a value of 0.6 was usually assumed, but see further discussion below), z is depth, ρgz is the lithostatic pressure and $\rho_w gz$ is the hydrostatic pressure.

The ductile parts of the yield-strength envelopes were assumed to be dominated by dislocation creep, following a power-law rheology:

$$\Delta\sigma = \left(\frac{\dot{\varepsilon}}{Ae^{-Q/RT}}\right)^{1/n}$$

where $\dot{\varepsilon}$ is the strain rate, A is the power-law stress constant, Q is the activation energy, n is the power-law exponent, R is the universal gas constant (8.3144621 J mol^{-1} K^{-1}) and T is the temperature

Table 1. *Density and thermal parameters assumed in the construction of the yield-strength envelopes*

Density and thermal parameters			
Rock unit	Density ($kg\ m^{-3}$)	Thermal conductivity ($W\ m^{-1}\ K^{-1}$)	Heat production ($\mu W\ m^{-3}$)
Sediments	2200	2.0	1.0
Crystalline crust	2850	2.5	1.0
HVLC	3000	2.5	0.3
Mantle	3300	*	0
Serpentinized mantle	3200	*	0

*Temperature-dependent thermal conductivity using the formulation of Xu *et al.* (2004) to define the lattice component and that of Hofmeister (1999) to define the radiative component (see also McKenzie *et al.* 2005).
HVLC, high-velocity lower crust (mafic).

in Kelvin. The parameters assumed for different lithologies are given in Table 2. A strain rate of $10^{-17}\ s^{-1}$ has been assumed, which is equivalent, for example, to a shortening of 0.5% over a period of 15 Ma. This is a higher rate than suggested by Gómez & Vergés (2005) for the Helland-Hansen Arch and the Vema Dome, but similar to that predicted by applying the shortening inferred by Vågnes *et al.* (1998) for the Ormen Lange Dome and the Helland-Hansen Arch over the timescales for the development of those structures indicated by Doré *et al.* (2008). The ductile behaviour of a range of possible crustal rocks has been simulated, ranging from weak (felsic and wet) to strong (mafic and dry). The filled parts of the strength envelopes shown in Figure 5 are based on a crust with the rheological properties of wet quartzite and a mantle with those of wet olivine, but the supplementary curves enable a range of alternatives to be visualized. For example, the effect of a mid-crustal lithological boundary can be assessed by drawing a horizontal line at the desired depth and adopting the curves for the preferred lithologies above and below that line.

Rheological behaviour of partially serpentinized upper mantle

Escartín *et al.* (2001) reported laboratory investigations into the strength of partially serpentinized peridotites. They concluded that the strength is not a simple function of the degree of serpentinization, but that there is an abrupt weakening at a serpentinite content of 10–15% or less (similar to the degree of serpentinization inferred to exist beneath the hyperextended basins on the NW European margin). The weakening is greater where the dominant serpentinite phase is lizardite rather than antigorite, and this is likely to be the case at temperatures below 300°C. Lizardite is progressively replaced by antigorite at higher temperatures, with the latter mineral becoming ubiquitous at 390°C and secondary olivine crystallization commencing at 460°C (Schwartz *et al.* 2013).

Experimental determinations of the coefficient of friction of lizardite typically lie in the range 0.3–0.5 (e.g. Escartín *et al.* 1997*b*), although lower values (0.15–0.35) have been reported by Reinen *et al.* (1994) and higher values (up to about 0.6)

Table 2. *Ductile deformation parameters assumed in the construction of the yield-strength envelopes*

Ductile deformation parameters (dislocation creep)				
Rock/mineral	A ($MPa^{-n}\ s^{-1}$)	n	Q ($kJ\ mol^{-1}$)	Source
Quartzite (wet)	1.1×10^{-4}	4	223	Burov & Watts (2006)
Diorite (wet)	3.8×10^{-2}	2.4	219	Carter & Tsenn (1987)
Felsic granulite	8×10^{-3}	3.1	243	Wilks & Carter (1990)
Mafic granulite	1.4×10^{4}	4.2	445	Wilks & Carter (1990)
Diabase (dry)	8	4.7	485	Burov & Watts (2006)
Olivine (wet)	417	4.48	498	Burov & Watts (2006)
Olivine (dry)	4.85×10^{4}	3.5	535	Burov & Watts (2006)
Antigorite	2.82×10^{-15}	3.8	8.9	Hilairet *et al.* (2007)

A, the power-law stress constant; n, the power-law exponent; Q, the activation energy.

by Moore *et al.* (1997). Chrysotile has a lower coefficient of friction than lizardite at room temperature, but this increases to similar values at around 200°C (Moore *et al.* 1997). Antigorite samples have higher friction coefficients, similar to those of unserpentinized rocks. There is a transition from localized to distributed (approximating to ductile) deformation in lizardite at around 200 MPa (depth of 9 km; Escartín *et al.* 1997*b*), although laboratory evidence suggests some pressure-dependence beyond this transition that can be simulated by assuming an appropriate coefficient of friction when calculating the yield-strength envelope. For example, the lizardite samples tested by Escartín *et al.* (1997*b*) lie along a trend equivalent to a friction coefficient of 0.3 at pressures of up to 950 MPa (depth of 33 km), and the partially serpentinized samples tested by Escartín *et al.* (2001) lie between the 0.3 and 0.5 coefficients at pressures of 300–450 MPa (depth of 12–17 km). Amiguet *et al.* (2012, 2014) reported weaker behaviour in high-pressure (1–8 GPa; 34–250 km depth) experiments on lizardite samples: they identified a strength under shear stress of about 100 MPa, with little pressure-dependence, associated with the dislocation glide of foliated lizardite along a basal plane. This weakening is dependent on crystal alignment, and a stronger rheology applies when the crystal orientation inhibits such glide (the locked geometry of Amiguet *et al.* 2012). Temperatures at these depths in the rheological models presented in this paper, however, lie outside the stability zone for lizardite (the experiments of Amiguet *et al.* (2012) were designed to simulate conditions in subduction zones).

To illustrate the potential influence of partial serpentinization on the yield-strength envelopes, alternative profiles are shown on the hyperextended example (Fig. 5e, f) for friction coefficients of 0.3, 0.4 and 0.5 in a zone extending from the Moho to the 400°C isotherm. From the above discussion, the most confidently identified zone of weakening is associated with lizardite and lies above the 300°C geotherm (shown in Fig. 5e, f). Below that, an increasing proportion of antigorite causes strengthening between 300 and 400°C, perhaps relatively rapidly if the effect is highly non-linear, as suggested by Escartín *et al.* (2001). A potential zone of lithospheric weakening is shown schematically with hachures in Figure 5e, f.

Hilairet *et al.* (2007) provided laboratory data for the deformation of antigorite, and observed a transition from brittle to ductile behaviour between 0.7 and 1 GPa (25–34 km). Their inferred power-law parameters (Table 2) indicate substantial weakening of antigorite below the brittle–ductile transition. If these parameters are included in a calculation for the partially serpentinized upper mantle using the aggregate flow laws of Tullis *et al.* (1991), a relatively high degree of serpentinization (30–40%) is required for the transition to appear in the envelopes (i.e. greater than indicated by seismic experiments). The problem with this approach is that it assumes that the phases are well dispersed, whereas interconnections of the serpentinite phase are likely to lead to greater weakening (Escartín *et al.* 2001). It follows that there is a zone between about 25 and 40 km (460°C) in the 'cool' hyperextended model in Figure 5e that might be weakened by ductile deformation of antigorite. With higher heat flow (Fig. 5f), the relevant pressures occur below the antigorite stability zone.

The present-day thickness and mineralogy of the zone of partial serpentinization will be a function of the conditions that applied when it was being formed (see Rüpke *et al.* 2013) and subsequent phase transformations. Simple sensitivity trials of the type illustrated here do not simulate the complexity of this process, but the zone of influence suggested for the 'cool' southern Rockall Basin example (Fig. 5e) is broadly compatible with the thickness of partial serpentinization indicated by seismic investigation (up to 10 km: O'Reilly *et al.* 2006). From the seismic evidence, it appears unlikely that the possible deeper zone of weakening associated with the ductile deformation of antigorite occurs below that basin, as normal upper-mantle velocities were encountered at depths of less than 25 km below seabed (O'Reilly *et al.* 2006). As an additional observation: the seismic velocity of antigorite lies between those of lizardite and normal upper mantle (Ji *et al.* 2013), so the lizardite–antigorite phase change may contribute to the velocity gradient seen at the base of the partially serpentinized zones.

Comparison of the yield-strength envelopes

The yield-strength envelopes provide only a general indication of strength variations within the lithosphere. In addition to the temperature uncertainties outlined above, the behaviour under stress is simulated using parameters derived from laboratory measurements on specimens at scales and strain rates that differ by many orders of magnitude from those that apply to the geological processes under consideration. The brittle predictions assume that the rock fails most readily along pre-existing, suitably orientated fractures, but under high-pressure conditions failure may occur more easily along new fractures (Zang *et al.* 2007; Pauselli *et al.* 2010). The transition from brittle to ductile behaviour probably involves semi-brittle failure at lower stresses than indicated by the 'spikes' in the yield-strength envelopes (Chester 1995; Kohlstedt *et al.* 1995). Despite these limitations, the envelopes are useful in identifying the sensitivity of lithospheric

strength to lithology and temperature, and the distribution of this strength in different regimes.

The yield-strength envelopes for 30 km-thick continental crust suggest that a 'jelly sandwich' strength profile may apply under cooler conditions (Fig. 5a); coupling between the strong layers will not occur unless there is thick and mafic mid to lower crust. As temperatures increase, the lithosphere is considerably weakened (Fig. 5b) through both the thickening of the ductile lower crust and the weakening of the upper mantle, to the extent that the lithospheric strength may reside solely in a relatively thin crustal layer ('crème brûlée' strength profile: Jackson 2002; Burov & Watts 2006).

Beneath the northern Rockall Basin (Fig. 5c, d), the predicted zone of strong upper mantle is thicker. There is likely to be coupling between crust and upper mantle at lower temperatures (Fig. 5c), but at higher temperatures decoupling may occur if the crust is relatively felsic and wet (Fig. 5d). The strong zone in the upper mantle beneath the southern Rockall Basin (Fig. 5e, f) extends to greater depth, and it appears unlikely that a ductile lower crust will develop under the range of temperatures simulated, regardless of the crustal composition. Although there is some lithospheric weakening as a result of partial serpentinization of the upper mantle, this zone is predicted to retain some strength and potentially maintain the coupling between the crust and mantle, at least under compression.

On the Norwegian margin, where a thick sedimentary layer overlies thin crystalline crust, a weak lower-crustal zone is likely to form if the crust is relatively felsic (Fig. 5g, h). Where high-velocity lower crust is present, and this is assumed to be due to mafic rocks (either high-grade basement or underplating), it will be stronger (Fig. 5i, j). If such a layer is interpreted as partially serpentinized upper mantle, the stress threshold for brittle deformation may be reduced as described above (a coefficient of friction of 0.4 is illustrated in Fig. 5i, j). With higher heat flows, which appear more likely in this area (Sundvor *et al.* 2000; Ritter *et al.* 2004), the predicted temperatures within this layer move out of the stability zone for lizardite (note the depths of the 300 and 400°C isotherms in Fig. 5j), so the likelihood of this being a source of weakening is reduced. The pressure in the layer is lower than the threshold for ductile deformation of antigorite identified by Hilairet *et al.* (2007).

Discussion

The information presented in Figures 3 and 4 suggests that there is not a consistent relationship between the siting of Cenozoic compressional structures on the NW European margin and zones where the crust had previously been hyperextended and the underlying mantle potentially serpentinized. While the Cenozoic domes in the Norwegian sector do lie in the vicinity of a hyperextended zone, the majority of Cenozoic inversion structures in the Faroe–Shetland–northern Rockall–Hatton area are located above crust that is less extended. There are fewer Cenozoic compressional structures in the southern Rockall and Porcupine basins, where hyperextension and serpentinization have been confidently identified.

Simple rheological models reveal the sensitivity of lithospheric strength to the thickness, composition and temperature of the crust. The weakest lithosphere occurs where the crust is felsic and thick, and the heat flow is high. This leads to a ductile lower crust overlain by a relatively thin upper-crustal brittle layer within which short-wavelength compressional structures may form. When stretching has occurred, its influence on the geothermal gradient is countered by the reduced crustal depth over which the gradient applies and a reduction in the influence of crustal heat production. This can lead to relatively strong (coupled) lithosphere where the stretching factor is high and there has been sufficient thermal re-equilibration. Partial serpentinization of the upper mantle weakens the lithosphere but, despite its non-linear nature (Escartín *et al.* 2001), does not necessarily lead to full decoupling between strong crust and strong upper mantle. This could explain the general lack of short-wavelength compressional structures over the southern Rockall and Porcupine basins, and also the lithospheric strength during sediment loading of those basins suggested by gravity anomalies (Kimbell *et al.* 2004).

In the Faroe–Shetland–northern Rockall–Hatton area, where serpentinization of the upper mantle appears less likely, lithospheric weakening and propensity to compressional deformation may be associated with the development of ductile lower crust. This is normally the case when the crust is relatively thick: however, in the more extended areas, relatively warm conditions would be required at the time of deformation. A thermal anomaly associated with the North Atlantic Igneous Province could have facilitated the development of the earlier (Paleocene–Eocene) structures. This is likely to be particularly relevant to the development of domes near the continent–ocean transition, and the presence of sill complexes of similar age in the basins along the margin indicates that the thermal anomaly extended further inboard. Its influence would, however, have reduced at the time of Neogene deformation. The Miocene and younger structures in the northern part of the Faroe–Shetland Basin are therefore more difficult to explain in this way, although there are some indications of a higher-temperature regime at that time in the results

of apatite fission track and vitrinite reflectance studies (e.g. Mark *et al.* 2008). Where a particularly strong thermal anomaly occurred, conditions could lie outside the range indicated in Figure 5, although a qualitative assessment of the impact can be made on the basis of extrapolation of the trends seen in that figure.

The criteria for appropriate conditions for the development of Cenozoic compressional structures in the Norwegian sector depend on the interpretation of the high-velocity lower crust (HVLC) identified there. If it is of mafic composition, weakening is most likely to have occurred where the overlying rock thickness (including the sedimentary layer) and geothermal gradient are large enough to allow a ductile zone to form above it. If the HVLC is actually partially serpentinized upper mantle, thin crust and/or a relatively low geothermal gradient may be a prerequisite for this layer to lie within the stability zone for lizardite. Higher temperatures would still weaken the lithosphere, through the thinning of the strong zone in the upper mantle and the potential development of a ductile layer in the overlying crust, but serpentinization could play a reduced role. The spatial relationship between the Cenozoic domes and the HVLC is inconclusive because there is overlap between these in the Vøring Basin but some divergence in the Møre Basin (Figs 4 & 6), although some spatial offset may be admissible if there was reactivation of low-angle detachments.

The contours in Figure 6 show the thickness of potentially weak crust in the Norwegian area, as measured from the seabed to the top of the HVLC, or to the Moho where HVLC was not detected. This version applies to the present day; the layer was up to 1–1.5 km thinner during the Miocene. Experimentation with mapping the temperature at the base of the potentially weak layer, which would be a more direct proxy for the presence of a weak zone, indicated a very similar pattern to that shown on the map, but required more assumptions that could distract from the simple point we wish to make. This is that the domes do not appear to have formed over the thinnest/coolest crust, but in an area where there is a general increase in the thickness of the potentially weak layer towards the east and SE, typically to more than 15 km. The 'Taper Break' of Redfield & Osmundsen (2013, 2014) lies just inboard of the compressional domes, and those authors related it to a concentration of earthquakes in that area. They argued that the earthquakes resulted from loading with Plio-Pleistocene glacial sediments (Byrkjeland *et al.* 2000) in combination with the relative weakening of the lithosphere by previous hyperextension, and used a flexed plate model to explain how locally derived bending stresses could generate the relatively deep ($>$15 km) compressive failure suggested by focal-plane solutions (Hicks *et al.* 2000). The hyperextended, weak lithosphere that extends oceanwards from this area was seen as 'protecting' it from the influence of far-field stresses. This (present-day) model does not appear to provide a full explanation for the earlier development of the Cenozoic domes, bearing in mind that they are upper-crustal structures with growth that is inferred to be due, at least in part, to far-field stresses. An alternative interpretation for the Norwegian domes is that the lithosphere outboard of them is strong (coupled) and thus aids the transmission of stresses originating from the oceanic area to the edge of a zone where weaker lithosphere facilitates deformation. The yield-strength profiles suggest that such coupling is feasible, given that the examples in Figure 5i, j coincide with the nominal 15 km 'threshold' for the thickness of the weak crustal layer and that this layer is thinner in the area in question. This hypothesis bears similarities to that of Mjelde *et al.* (2003, 2005) in which the distribution of compressional structures was influenced by rigid blocks underlain by HVLC. There is a possible analogue on the Hatton margin, where the compressional structures lie just inboard of the approximately 40 km-wide zone adjacent to the ocean margin affected by mafic intrusion (Johnson *et al.* 2005; White & Smith 2009).

Péron-Pinvidic *et al.* (2008) observed a correlation between a zone underlain by shallow, highly serpentinized exhumed continental mantle and Cenozoic compressional deformation on the Iberian margin, and concluded that this was the weakest zone on that margin. The estimated degree of serpentinization is 60–100% in the top 2–3 km of the upper mantle and 25–45% in the underlying layer, with a gradual transition to normal mantle values at depths of about 10 km below seabed (Chian *et al.* 1999). Landwards of this is a zone of hyperextended continental crust (2–5 km thick) underlain by a layer with a P-wave velocity of 7.3–7.9 km s^{-1}, which was interpreted as weakly serpentinized ($<$25%) upper mantle (Chian *et al.* 1999). Cenozoic deformational structures are rare in this zone. The geotherms beneath the two areas are unlikely to differ substantially, since the observed heat flow is similar (Louden *et al.* 1997) and the presence of a large proportion of lizardite will reduce the thermal conductivity of the highly serpentinized upper mantle to values closer to that of continental crust (Horai 1971). Brittle deformation is likely to dominate at the depths where the lateral strength contrasts are greatest, so it is the low effective coefficient of friction in the highly serpentinized upper mantle (and particularly in fault zones within this layer?) that is likely to explain the weakening. The degree of serpentinization beneath the

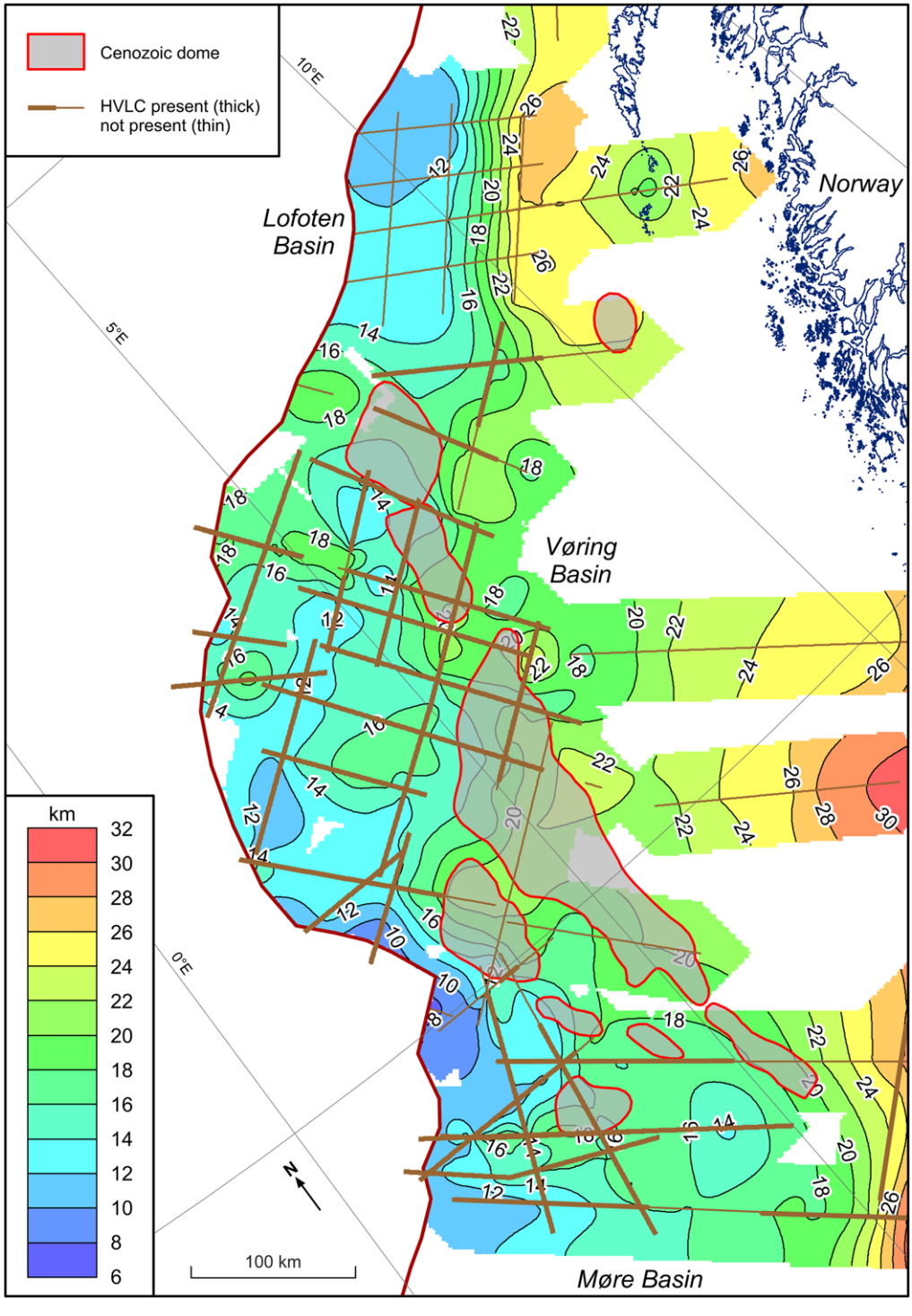

Fig. 6. Locations of Cenozoic domes and high-velocity lower crust (HVLC) on the Norwegian margin superimposed on a contour map of the thickness of potentially weak continental crust (i.e. measured from the seabed to the top of the HVLC). Contours are at 2 km intervals.

hyperextended areas on the NW European margin is closer to that of the stronger zone on the Iberian margin, so the latter margin does not provide an effective analogue for a general relationship between partial serpentinization and compressional deformation further north.

The way in which the lithosphere was stretched during the Mesozoic will have influenced the likelihood of both upper-mantle serpentinization and, consequently, its Cenozoic strength profile. Where the upper part of the crust is extended more than the lower part, its heat production (which is typically concentrated in the upper crust) will be strongly attenuated, leading to a reduction in lower-crustal temperatures and a greater likelihood of embrittlement (and, thus, water ingress and serpentinization). If stretching increases with depth, the cooling effect will be smaller and may not be sufficient for embrittlement to occur. Such a contrast in stretching style may explain the presence of serpentinized upper mantle beneath the southern Rockall and Porcupine basins (Hauser *et al.* 1995; O'Reilly *et al.* 1996, 2006), and its absence beneath the Orphan Basin on the Eastern Canadian conjugate margin, where stretching factors are similar (Welford *et al.* 2012). In the Cenozoic strength profiles, the lower temperatures in the former case reduces the likelihood of ductile lower crust developing above the serpentinized zone (although this may be offset by the thermal blanketing effect of a subsequently deposited, thick sedimentary sequence).

Reactivation of Mesozoic extensional structures provides control over the siting of at least some of the Cenozoic domes observed along the margin. In some cases, this relationship can be seen in seismic reflection data (e.g. the examples shown in Fig. 2a, e, f), but elsewhere it is inferred rather than proven because of difficulties with imaging basin architecture beneath Palaeogene igneous rocks (Doré *et al.* 2008). Reactivation provides a possible explanation for the siting of compressional structures in the areas where the predicted lithospheric strength does not appear optimum: for example, within basins rather than over the thicker crust on their flanks. Van Wees & Beekman (2000) reconstructed the rheological evolution of several basins that have undergone inversion and found evidence for strengthening rather than weakening at the time of inversion, relative to initial values; they concluded that the susceptibility to inversion was explained by pre-existing weak zones. Upper-crustal failure related to fault reactivation indicates that the orientation and frictional resistance of a fault zone can result in it failing more readily than the neighbouring rock mass, with fluid overpressure being an important factor, as well as the lithology of the fault gouge (Sibson 1995; Turner & Williams 2004). At depth, faults may detach into ductile lower crust or partially serpentinized upper mantle, depending on the setting. In the latter case, the weakening will be enhanced if there are appropriately orientated major structures containing foliated lizardite aligned such that dislocation glide is facilitated. Fluid overpressure may be enhanced in such zones as a result of water produced by the dehydration of the serpentine minerals (Raleigh & Paterson 1965).

As well as specific examples of reactivation, there is a more general relationship between groups of compressional structures and the boundaries between the Vøring and Møre basins in the north and the Faroe–Shetland and northern Rockall basins in the south. The implication is that the complex of structures that facilitated the transfer of Mesozoic extension within and between these basins also created preferential sites for compressional reactivation. The Mogdunn Arch, South Mogdunn Arch, Havsule Dome and Ormen Lange Dome are arrayed along the northern of the two transfer zones (Doré *et al.* 2008), and the Wyville Thomson Ridge and Ymir Ridge may correspond to reactivation of individual strands within the southern one (Kimbell *et al.* 2005).

Temporal and spatial variations in the stress field have to be taken into account when considering the spatial distribution of compressional structures. Although the growth histories of the observed folds are complex, in broad terms two dominant phases can be identified: one in the Palaeogene (most commonly the Eocene) and one in the Neogene (dominantly in the Miocene). This is illustrated, for example, by the chronological charts of Doré *et al.* (2008, fig. 4) and Ritchie *et al.* (2008, fig. 3). Although the influence of transient thermal weakening at these times may be a contributing factor, temporal variations in the stress field are a likely primary explanation for this timing. The stress regime is the result of multiple influences, including ridge-push and other plate-boundary forces, mantle drag, and Alpine/Pyrenean/Eurekan orogenic stresses. These will not be discussed in detail here (see the useful review by Doré *et al.* 2008), except to acknowledge that the propensity of a particular area to compressional deformation at a particular time will depend on local stress magnitude and orientation, as well as lithospheric rheology and the availability of suitably orientated pre-existing structures. Compressional stresses generated by differences in gravitational potential energy (GPE), including those associated with the Miocene growth of the Iceland Insular Margin (Doré *et al.* 2008) and the influence of the Southern Scandes (Pascal & Cloetingh 2009), will be greatest in areas of low GPE, possibly contributing to the development of compressional structures in deeper basinal settings. Plate break-up adjacent to the Faroe–Shetland–north Rockall area was complex and protracted,

and included the separation and rotation of the Jan Mayen microcontinent; this may have generated stresses that contributed to the concentration of compressional structures in that area (Stoker *et al.* 2013). Borehole breakouts in the Faroe–Shetland Basin indicate that the contemporary maximum horizontal compressive stress is orientated approximately NW–SE in the northern part of the basin, but that more variable stress orientations occur in its central and SW parts, and these have been interpreted in terms of deflections towards weak faults (Holford *et al.* 2016). This is compatible with the basin-parallel trends of compressional structures in the north of the basin, and variable trends of the Judd and Westray anticlines in the south.

An example of susceptibility to compressional deformation changing with time is provided by the two sections in the southern part of the area illustrated in Figure 2e, f. Pre-latest Eocene deformation is observed in the central part of the Rockall Basin (Fig. 2e), but there is little evidence of short-wavelength deformation in the rocks overlying the Late Eocene unconformity here or elsewhere in the southern Rockall Basin. However, the example from the Colmán Basin (Fig. 2f) illustrates that similarly orientated short-wavelength compressional deformation did occur at these later times, at a nearby location where the crust is thicker and upper-mantle serpentinization less likely. The implication is that the hyperextended lithosphere of the southern Rockall Basin has strengthened with time. If such strengthening is due to cooling, it can be correlated with the thickening of strong (coupled) lithosphere, as illustrated in the 'warm' and 'cool' examples in Figure 5f, e, respectively. It is unlikely to relate to a change in the thickness and mineralogy of the partially serpentinized zone, given the relationship between temperature and the stability of the serpentine minerals, but might be assisted by the loss of transient overpressure associated with earlier dehydration.

The emphasis in the discussion so far has been on the development of short-wavelength ($<c.$ 100 km) compressional structures. Longer-wavelength (hundreds of km) deformation is evident along the NW European margin, in particular as regional 'sagging' at the end of the Eocene and intra-Pliocene 'tilting' (Praeg *et al.* 2005; Stoker *et al.* 2005*b*). Long-wavelength lithospheric folds can form as a result of in-plane compressive stresses and this can occur coevally with the development of short-wavelength structures in rheologically stratified lithosphere, with the former associated with the deformation of strong upper mantle and the latter with deformation of decoupled upper crust (Cloetingh *et al.* 1999; Cloetingh *et al.* 2008; Cloetingh & Burov 2011). Numerical modelling is required to test whether the observed long-wavelength features are reproducible by in-plane stress, and this topic is not considered in the present paper. Previous modelling has suggested amplitudes of hundreds of metres rather than the observed kilometre-scale 'sagging' and 'tilting' of Stoker *et al.* (2005*b*) and Praeg *et al.* (2005), leading those authors to prefer an alternative mechanism involving shallow mantle convection.

Conclusions

- A comparison between the locations of Cenozoic compressional structures on the NW European margin and regional lithospheric models produced by the NAG-TEC project (Hopper *et al.* 2014) suggests that there is not a simple relationship between the distribution of the structures and the degree of Mesozoic lithospheric stretching. In particular, an association with areas of hyperextension and partial serpentinization of the upper mantle, as proposed by Lundin & Doré (2011), is not consistently observed. The strongest evidence for such an association occurs on the Norwegian margin, but there is little support for it in the southern Rockall Basin where a well-resolved zone of partially serpentinized upper mantle is overlain by largely undeformed Cenozoic strata.
- A range of compressional structures formed in the Faroe–Shetland–northern Rockall area during the Cenozoic. Although the lithosphere in parts of this area (the deepest parts of the Faroe–Shetland and northern Rockall basins) has undergone substantial extension, current evidence suggests that the amount of stretching is insufficient to have resulted in upper-mantle serpentinization. The data are sparse, but there is as yet no indication of reduced upper-mantle velocities that would be indicative of such serpentinization. These conclusions are particularly tentative in the northern Faroe–Shetland Basin, where the deep structure is poorly understood.
- Rheological modelling reveals the sensitivity of the strength of the lithosphere to crustal configuration, lithological variation and temperature profile. The modelling has not been used to address the state of the lithosphere during Mesozoic extension (for this see, e.g., Pérez-Gussinyé & Reston 2001; Rüpke *et al.* 2013), but rather to consider conditions that may have applied later, during Cenozoic compression. Even so, the uncertainties in this modelling are such that it is only used to provide some rheological context for the observed spatial distributions rather than make detailed predictions.
- There are particular uncertainties in modelling the rheology of partially serpentinized upper mantle, but the current results suggest that

conflicting factors affect the degree of lithospheric weakening associated with the presence of such a zone. Lower temperatures promote the stability of the serpentine minerals, but also lead to a thickening of underlying strong upper mantle, which may be coupled to a strong crust, depending on the effective coefficient of friction of the intervening, partially serpentinized zone. Alignment of lizardite crystals and fluid overpressure in fault zones could lead to enhanced weakening, and the overpressure could be a transient phenomenon that only applied during a particular phase of basin evolution.

- In areas where short-wavelength compressional structures occur and serpentinized upper mantle is not present, thermally related lithospheric weakening, involving decoupling by ductile lower crust, may have facilitated their development.
- Although (or, perhaps, because) it is the most thoroughly investigated part of the study area, the Norwegian margin is the most controversial in terms of its deep structure and, in particular, whether the high-velocity lower crust (HVLC) there is of magmatic or metamorphic origin, or is associated with partially serpentinized upper mantle. The weakening implicit in the latter interpretation is compatible with the development of overlying compressional structures, but the spatial relationships admit an alternative interpretation in which the domes formed at the edge of a rheologically weaker zone against a 'buttress' underpinned by mafic (metamorphic or igneous) lower crust. More detailed investigation is required, involving the development of alternative lithological and rheological models along selected deep seismic profiles, flexural/gravity modelling to investigate spatial variations in lithospheric strength indicated by the response to sediment loading, and numerical simulation of the effect of compression on the alternative models.
- Rheological modelling can help in understanding the general factors that influence the propensity of an area to compressional deformation, but these are complemented (and may be outweighed) by the presence of specific weak zones associated with pre-existing structures.

This study has employed the results of the NAG-TEC project, and we acknowledge the support of the industry sponsors of that project (in alphabetical order): Bayerngas Norge AS; BP Exploration Operating Company Limited, Bundesanstalt für Geowissenschaften und Rohstoffe (BGR); Chevron East Greenland Exploration A/S; ConocoPhillips Skandinavia AS; DEA Norge AS; Det norske oljeselskap ASA; DONG E&P A/S; E.ON Norge AS; ExxonMobil Exploration and Production Norway AS; Japan Oil, Gas and Metals National Corporation (JOGMEC); Maersk Oil; Nalcor Energy – Oil and Gas Inc.; Nexen Energy ULC, Norwegian Energy Company ASA (Noreco); Repsol Exploration Norge AS; Statoil (U.K.) Limited and Wintershall Holding GmBH. We are very grateful to Mick Hanrahan at the Irish Petroleum Affairs Division of the Department of Communications, Energy and Natural Resources for his assistance with the permission to publish Figure 2f. The contribution of Kimbell, Stewart and Stoker is made with the permission of the Executive Director of the British Geological Survey (Natural Environment Research Council).

References

Amiguet, E., Reynard, B., Caracas, R., Van de Moortèle, B., Hilairet, N. & Wang, Y. 2012. Creep of phyllosilicates at the onset of plate tectonics. *Earth and Planetary Science Letters*, **345–348**, 142–150, https://doi.org/10.1016/j.epsl.2012.06.033

Amiguet, E., Van De Moortele, B., Reynard, B., Cordier, P. & Hilairet, N. 2014. Deformation mechanisms and rheology of serpentines in experiments and in nature. *Journal of Geophysical Research*, **119**, 4640–4655, https://doi.org/10.1002/2013JB010791

Anderson, E.M. 1951. *The Dynamics of Faulting and Dyke Formation with Applications to Britain*. Oliver & Boyd, Edinburgh.

Archer, S.G., Bergman, S.C., Iliffe, J., Murphy, C.M. & Thornton, M. 2005. Palaeogene igneous rocks reveal new insights into the geodynamic evolution and petroleum potential of the Rockall Trough, NE Atlantic Margin. *Basin Research*, **17**, 171–201, https://doi.org/10.1111/j.1365-2117.2005.00260.x

Barton, A.J. & White, R.S. 1997. Crustal structure of Edoras Bank continental margin and mantle thermal anomalies beneath the North Atlantic. *Journal of Geophysical Research: Solid Earth*, **102**, 3109–3129, https://doi.org/10.1029/96jb03387

Blystad, P., Brekke, H., Frerseth, R.B., Larsen, B.T., Skogseid, J. & Tørudbakken, B. 1995. *Structural Elements of the Norwegian Continental Shelf. Part 2: The Norwegian Sea Region*. Norwegian Petroleum Directorate Bulletin, **8**.

Boldreel, L.O. & Andersen, M.S. 1993. Late Paleocene to Miocene compression in the Faroe–Rockall area. *In*: Parker, J.R. (ed.) *Petroleum Geology of NW Europe: Proceedings of the 4th Conference*. Geological Society, London, 1025–1034, https://doi.org/10.1144/0041025

Boldreel, L.O. & Andersen, M.S. 1995. The relationship between the distribution of Tertiary sediments, tectonic processes and deep-water circulation around the Faeroe Islands. *In*: Scrutton, R.A., Stoker, M.S., Shimmield, G.B. & Tudhope, A.W. (eds) *The Tectonics, Sedimentation and Palaeoceanography of the North Atlantic Region*. Geological Society, London, Special Publications, **90**, 145–158, https://doi.org/10.1144/gsl.sp.1995.090.01.09

Boldreel, L.O. & Andersen, M.S. 1998. Tertiary compressional structures on the Faroe–Rockall Plateau in relation to northeast Atlantic ridge-push and Alpine foreland stresses. *Tectonophysics*, **300**, 13–28, https://doi.org/10.1016/s0040-1951(98)00231-5

Bott, M.H.P., Armour, A.R., Himsworth, E.M., Murphy, T. & Wylie, G. 1979. Explosion seismology investigation of the continental-margin west of the Hebrides, Scotland, at 58°N. *Tectonophysics*, **59**, 217–231, https://doi.org/10.1016/0040-1951(79)90046-5

Brekke, H. 2000. The tectonic evolution of the Norwegian Sea Continental Margin with emphasis on the Vøring and Møre Basins. *In*: Nøttvedt, A. (ed.) *Dynamics of the Norwegian Margin*. Geological Society, London, Special Publications, **167**, 327–378, https://doi.org/10.1144/GSL.SP.2000.167.01.13

Burov, E.B. 2011. Rheology and strength of the lithosphere. *Marine and Petroleum Geology*, **28**, 1402–1443, https://doi.org/10.1016/j.marpetgeo.2011.05.008

Burov, E.B. & Watts, A.B. 2006. The long-term strength of continental lithosphere: 'jelly sandwich' or 'crème brûlée'? *GSA Today*, **16**, 4–10.

Byrkjeland, U., Bungum, H. & Eldholm, O. 2000. Seismotectonics of the Norwegian continental margin. *Journal of Geophysical Research*, **105**, 6221–6236, https://doi.org/10.1029/1999JB900275

Carter, N.L. & Tsenn, M.C. 1987. Flow properties of continental lithosphere. *Tectonophysics*, **136**, 27–63, https://doi.org/10.1016/0040-1951(87)90333-7

Chester, F.M. 1995. A rheologic model for wet crust applied to strike-slip faults. *Journal of Geophysical Research*, **100**, 13,033–13,044, https://doi.org/10.1029/95JB00313

Chian, D.P., Louden, K.E., Minshull, T.A. & Whitmarsh, R.B. 1999. Deep structure of the ocean-continent transition in the southern Iberia Abyssal Plain from seismic refraction profiles: Ocean Drilling Program (Legs 149 and 173) transect. *Journal of Geophysical Research*, **104**, 7443–7462, https://doi.org/10.1029/1999JB900004

Christensen, N.I. 2004. Serpentinites, peridotites, and seismology. *International Geology Review*, **46**, 795–816, https://doi.org/10.2747/0020-6814.46.9.795

Cloetingh, S. & Burov, E. 2011. Lithospheric folding and sedimentary basin evolution: a review and analysis of formation mechanisms. *Basin Research*, **23**, 257–290, https://doi.org/10.1111/j.1365-2117.2010.00490.x

Cloetingh, S., Burov, E. & Poliakov, A. 1999. Lithosphere folding: primary response to compression? (from central Asia to Paris basin). *Tectonics*, **18**, 1064–1083, https://doi.org/10.1029/1999TC900040

Cloetingh, S., Beekman, F., Ziegler, P.A., van Wees, J.-D. & Sokoutis, D. 2008. Post-rift compressional reactivation potential of passive margins and extensional basins. *In*: Johnson, H., Doré, A.G., Gatliff, R.W., Holdsworth, R., Lundin, E.R. & Ritchie, J.D. (eds) *The Nature and Origin of Compression in Passive Margins*. Geological Society, London, Special Publications, **306**, 27–70, https://doi.org/10.1144/sp306.2

Davies, R., Cloke, I., Cartwright, J., Robinson, A. & Ferrero, C. 2004. Post-breakup compression of a passive margin and its impact on hydrocarbon prospectivity: an example from the Tertiary of the Faroe–Shetland Basin, United Kingdom. *American Association of Petroleum Geologists Bulletin*, **88**, 1–20.

Davies, R.J. & Cartwright, J. 2002. A fossilized Opal A to Opal C/T transformation on the northeast Atlantic margin: support for a significantly elevated palaeogeothermal gradient during the Neogene? *Basin Research*, **14**, 467–486, https://doi.org/10.1046/j.1365-2117.2002.00184.x

Doré, A.G., Lundin, E.R., Jensen, L.N., Birkeland, O., Eliassen, P.E. & Fichler, C. 1999. Principal tectonic events in the evolution of the northwest European Atlantic margin. *In*: Fleet, A.J. & Boldy, S.A.R. (eds) *Petroleum Geology of Northwest Europe: Proceedings of the 5th Conference*. Geological Society, London, 41–61, https://doi.org/10.1144/0050041

Doré, A.G., Lundin, E.R., Kusznir, N.J. & Pascal, C. 2008. Potential mechanisms for the genesis of Cenozoic domal structures on the NE Atlantic margin: pros, cons and some new ideas. basins. *In*: Johnson, H., Doré, A.G., Gatliff, R.W., Holdsworth, R., Lundin, E.R. & Ritchie, J.D. (eds) *The Nature and Origin of Compression in Passive Margins*. Geological Society, London, Special Publications, **306**, 1–26, https://doi.org/10.1144/sp306.1

Ebbing, J. 2007. Isostatic density modelling explains the missing root of the Scandes. *Norwegian Journal of Geology*, **87**, 13–20.

Ebbing, J., Lundin, E., Olesen, O. & Hansen, E.K. 2006. The mid-Norwegian margin: a discussion of crustal lineaments, mafic intrusions, and remnants of the Caledonian root by 3D density modelling and structural interpretation. *Journal of the Geological Society, London*, **163**, 47–59, https://doi.org/10.1144/0016-764905-029

Escartín, J., Hirth, G. & Evans, B. 1997*a*. Effects of serpentinization on the lithospheric strength and the style of normal faulting at slow-spreading ridges. *Earth and Planetary Science Letters*, **151**, 181–189, https://doi.org/10.1016/S0012-821X(97)81847-X

Escartín, J., Hirth, G. & Evans, B. 1997*b*. Nondilatant brittle deformation of serpentinites: implications for Mohr-Coulomb theory and the strength of faults. *Journal of Geophysical Research*, **102**, 2897–2913, https://doi.org/10.1029/96JB02792

Escartín, J., Hirth, G. & Evans, B. 2001. Strength of slightly serpentinized peridotites: implications for the tectonics of oceanic lithosphere. *Geology*, **29**, 1023–1026, https://doi.org/10.1130/0091-7613(2001)029<1023:SOSSPI>2.0.CO;2

Funck, T., Andersen, M.S., Neish, J.K. & Dahl-Jensen, T. 2008. A refraction seismic transect from the Faroe Islands to the Hatton–Rockall Basin. *Journal of Geophysical Research*, **113**, B12405, https://doi.org/10.1029/2008JB005675

Funck, T., Hopper, J.R. *et al*. 2014. Crustal structure. *In*: Hopper, J.R., Funck, T., Stoker, M., Árting, U., Péron-Pinvidic, G., Doornenbal, H. & Gaina, C. (eds) *NAG-TEC Atlas: Tectonostratigraphic Atlas of the North-East Atlantic Region*. Geological Survey of Denmark and Greenland (GEUS), Copenhagen, 69–126.

Funck, T., Geissler, W.H., Kimbell, G.S., Gradmann, S., Erlendsson, Ö., McDermott, K. & Petersen, U.K. In press. Moho and basement depth in the NE Atlantic Ocean based on seismic refraction data and receiver functions. *In*: Péron-Pinvidic, G., Hopper,

J.R., Stoker, M.S., Gaina, C., Doornenbal, J.C., Funck, T. & Árting, U.E. (eds) *The NE Atlantic Region: A Reappraisal of Crustal Structure, Tectonostratigraphy and Magmatic Evolution*. Geological Society, London, Special Publications, **447**, https://doi.org/10.1144/SP447.1

Gernigon, L., Ringenbach, J.C., Planke, S., Le Gall, B. & Jonquet-Kolsto, H. 2003. Extension, crustal structure and magmatism at the outer Vøring Basin, Norwegian margin. *Journal of the Geological Society, London*, **160**, 197–208, https://doi.org/10.1144/0016-764902-055

Gernigon, L., Ringenbach, J.C., Planke, S. & Le Gall, B. 2004. Deep structures and breakup along volcanic rifted margins: insights from integrated studies along the outer Vøring Basin (Norway). *Marine and Petroleum Geology*, **21**, 363–372, https://doi.org/10.1016/j.marpetgeo.2004.01.005

Gómez, M. & Vergés, J. 2005. Quantifying the contribution of tectonics v. differential compaction in the development of domes along the Mid-Norwegian Atlantic margin. *Basin Research*, **17**, 289–310, https://doi.org/10.1111/j.1365-2117.2005.00264.x

Haase, C., Ebbing, J. & Funck, T. In review. A 3D regional crustal model of the Northeast Atlantic based on seismic and gravity data. *In*: Péron-Pinvidic, G., Hopper, J.R., Stoker, M.S., Gaina, C., Doornenbal, J.C., Funck, T. & Árting, U.E. (eds) *The NE Atlantic Region: A Reappraisal of Crustal Structure, Tectonostratigraphy and Magmatic Evolution*. Geological Society, London, Special Publications, **447**.

Hauser, F., O'Reilly, B.M., Jacob, A.W.B., Shannon, P.M., Makris, J. & Vogt, U. 1995. The crustal structure of the Rockall Trough: differential stretching without underplating. *Journal of Geophysical Research*, **100**, 4097–4116, https://doi.org/10.1029/94jb02879

Hicks, E.C., Bungum, H. & Lindholm, C.D. 2000. Stress inversion of earthquake focal mechanism solutions from onshore and offshore Norway. *Norsk Geologisk Tidsskrift*, **80**, 235–250.

Hilairet, N., Reynard, B., Wang, Y., Daniel, I., Merkel, S., Nishiyama, N. & Petitgirard, S. 2007. High-pressure creep of serpentine, interseismic deformation, and initiation of subduction. *Science*, **318**, 1910–1913, https://doi.org/10.1126/science.1148494

Hitchen, K. 2004. The geology of the UK Hatton-Rockall margin. *Marine and Petroleum Geology*, **21**, 993–1012, https://doi.org/10.1016/j.marpetgeo.2004.05.004

Hodges, S., Line, C. & Evans, R. 1999. The other millennium dome. Paper SPE 56895 presented at the *Society of Petroleum Engineers, Offshore Europe Oil and Gas Exhibition and Conference*, 7–10 September 1999, Aberdeen, UK.

Hofmeister, A.M. 1999. Mantle values of thermal conductivity and the geotherm from phonon lifetimes. *Science*, **283**, 1699–1706, https://doi.org/10.1126/science.283.5408.1699

Holford, S.P., Tassone, D.R., Stoker, M.S. & Hillis, R.R. 2016. Contemporary stress orientations in the Faroe–Shetland region. *Journal of the Geological Society, London*, **173**, 142–152, https://doi.org/10.1144/jgs2015-048

Holmes, R., Hobbs, P.R.N. *et al.* 2003. *DTI Strategic Environmental Assessment Area 4 (SEA4): Geological Evolution Pilot Whale Diapirs and Stability of the Seabed Habitat*. British Geological Survey Commissioned Report, CR/03/082. British Geological Survey, Nottingham, UK.

Hopper, J.R. & Buck, W.R. 1998. Styles of extensional decoupling. *Geology*, **26**, 699–702, https://doi.org/10.1130/0091-7613(1998)026<0699:SOED>2.3.CO;2

Hopper, J.R., Funck, T., Stoker, M., Árting, U., Peron-Pinvidic, G., Doornenbal, H. & Gaina, C. (eds). 2014. *NAG-TEC Atlas: Tectonostratigraphic Atlas of the North-East Atlantic Region*. Geological Survey of Denmark and Greenland (GEUS), Copenhagen.

Hopper, J.R., Fatah, R.A., Gaina, C., Geissler, W., Doornenbal, H., Funck, T. & Kimbell, G.S. In prep. Sediment thickness and residual topography of the North Atlantic: estimating dynamic topography around Iceland. *In*: Péron-Pinvidic, G., Hopper, J.R., Stoker, M.S., Gaina, C., Doornenbal, J.C., Funck, T. & Árting, U.E. (eds) *The NE Atlantic Region: A Reappraisal of Crustal Structure, Tectonostratigraphy and Magmatic Evolution*. Geological Society, London, Special Publications, **447**.

Horai, K. 1971. Thermal conductivity of rock-forming minerals. *Journal of Geophysical Research*, **76**, 1278–1308, https://doi.org/10.1029/JB076i005 p01278

Jackson, J. 2002. Strength of the continental lithosphere: time to abandon the jelly sandwich? *GSA Today*, **12**, 4–9.

Jacob, A.W.B., Kaminski, W., Murphy, T., Phillips, W.E.A. & Prodehl, C. 1985. A crustal model for a northeast-southwest profile through Ireland. *Tectonophysics*, **113**, 75–103, https://doi.org/10.1016/0040-1951(85)90111-8

Ji, S., Li, A., Wang, Q., Long, C., Wang, H., Marcotte, D. & Salisbury, M. 2013. Seismic velocities, anisotropy, and shear-wave splitting of antigorite serpentinites and tectonic implications for subduction zones. *Journal of Geophysical Research*, **118**, 1015–1037, https://doi.org/10.1002/jgrb.50110

Johnson, H., Ritchie, J.D., Hitchen, K., McInroy, D.B. & Kimbell, G.S. 2005. Aspects of the Cenozoic deformational history of the northeast Faroe–Shetland Basin, Wyville–Thomson Ridge and Hatton Bank areas. *In*: Doré, A.G. & Vining, B.A. (eds) *Petroleum Geology: North-West Europe and Global Perspectives – Proceedings of the 6th Petroleum Geology Conference*. Geological Society, London, 993–1007, https://doi.org/10.1144/0060993

Joppen, M. & White, R.S. 1990. The structure and subsidence of Rockall Trough from two-ship seismic experiments. *Journal of Geophysical Research: Solid Earth*, **95**, 19821–19837, https://doi.org/10.1029/JB095iB12p19821

Kimbell, G.S., Gatliff, R.W., Ritchie, J.D., Walker, A.S.D. & Williamson, J.P. 2004. Regional three-dimensional gravity modelling of the NE Atlantic margin. *Basin Research*, **16**, 259–278, https://doi.org/10.1111/j.1365-2117.2004.00232.x

Kimbell, G.S., Ritchie, J.D., Johnson, H. & Gatliff, R.W. 2005. Controls on the structure and evolution of the NE Atlantic margin revealed by regional

potential field imaging and 3D modelling. *In*: Doré, A.G. & Vining, B.A. (eds) *Petroleum Geology: North-West Europe and Global Perspectives – Proceedings of the 6th Petroleum Geology Conference*. Geological Society, London, 933–945, https://doi.org/10.1144/0060933

Klingelhöfer, F., Edwards, R.A., Hobbs, R.W. & England, R.W. 2005. Crustal structure of the NE Rockall Trough from wide-angle seismic data modeling. *Journal of Geophysical Research*, **110**, B11105, https://doi.org/10.1029/2005JB003763

Kohlstedt, D.L., Evans, B. & Mackwell, S.J. 1995. Strength of the lithosphere: constraints imposed by laboratory experiments. *Journal of Geophysical Research*, **100**, 17,587–17,602, https://doi.org/10.1029/95JB01460

Kvarven, T., Ebbing, J. *et al.* 2014. Crustal structure across the Møre margin, mid-Norway, from wide-angle seismic and gravity data. *Tectonophysics*, **626**, 21–40, https://doi.org/10.1016/j.tecto.2014.03.021

Louden, K.E., Sibuet, J.C. & Harmegnies, F. 1997. Variations in heat flow across the ocean-continent transition in the Iberia abyssal plain. *Earth and Planetary Science Letters*, **151**, 233–254, https://doi.org/10.1016/S0012-821X(97)81851-1

Lowe, C. & Jacob, A.W.B. 1989. A north-south seismic profile across the Caledonian Suture zone in Ireland. *Tectonophysics*, **168**, 297–318, https://doi.org/10.1016/0040-1951(89)90224-2

Lundin, E.R. & Doré, A.G. 2002. Mid-Cenozoic post-breakup deformation in the 'passive' margins bordering the Norwegian-Greenland Sea. *Marine and Petroleum Geology*, **19**, 79–93, https://doi.org/10.1016/s0264-8172(01)00046-0

Lundin, E.R. & Doré, A.G. 2011. Hyperextension, serpentinization, and weakening: a new paradigm for rifted margin compressional deformation. *Geology*, **39**, 347–350, https://doi.org/10.1130/g31499.1

Lundin, E.R., Doré, A.G., Rønning, K. & Kyrkjebø, R. 2013. Repeated inversion and collapse in the Late Cretaceous–Cenozoic northern Vøring Basin, offshore Norway. *Petroleum Geoscience*, **19**, 329–341, https://doi.org/10.1144/petgeo2012-022

Makris, J., Papoulia, I. & Ziska, H. 2009. Crustal structure of the Shetland–Faeroe Basin from long offset seismic data. *In*: Varming, T. & Ziska, H. (eds) *Faroe Island Exploration Conference: Proceedings of the 2nd Conference*. Faroese Academy of Sciences, Tórshavn, 30–42.

Mark, D.F., Green, P.F., Parnell, J., Kelley, S.P., Lee, M.R. & Sherlock, S.C. 2008. Late Palaeozoic hydrocarbon migration through the Clair field, West of Shetland, UK Atlantic margin. *Geochimica et Cosmochimica Acta*, **72**, 2510–2533, https://doi.org/10.1016/j.gca.2007.11.037

Masson, D.G. & Parson, L.M. 1983. Eocene deformation on the continental margin SW of the British Isles. *Journal of the Geological Society, London*, **140**, 913–920, https://doi.org/10.1144/gsjgs.140.6.0913

McDonnell, A. & Shannon, P.M. 2001. Comparative Tertiary stratigraphic evolution of the Porcupine and Rockall basins. *In*: Shannon, P.M., Haughton, P.D.W. & Corcoran, D.V. (eds) *The Petroleum Exploration of Ireland's Offshore Basins*. Geological Society, London, Special Publications, **188**, 323–344, https://doi.org/10.1144/GSL.SP.2001.188.01.19.

McKenzie, D. 1978. Some remarks on the development of sedimentary basins. *Earth and Planetary Science Letters*, **40**, 25–32, https://doi.org/10.1016/0012-821X(78)90071-7

McKenzie, D., Jackson, J. & Priestley, K. 2005. Thermal structure of oceanic and continental lithosphere. *Earth and Planetary Science Letters*, **233**, 337–349, https://doi.org/10.1016/j.epsl.2005.02.005

Minshull, T.A. 2009. Geophysical characterisation of the ocean–continent transition at magma-poor rifted margins. *Comptes Rendus Geoscience*, **341**, 382–393, https://doi.org/10.1016/j.crte.2008.09.003

Mjelde, R., Kodaira, S., Shimamura, H., Kanazawa, T., Shiobara, H., Berg, E.W. & Riise, O. 1997. Crustal structure of the central part of the Vøring Basin, mid-Norway margin, from ocean bottom seismographs. *Tectonophysics*, **277**, 235–257, https://doi.org/10.1016/S0040-1951(97)00028-0

Mjelde, R., Kasahara, J. *et al.* 2002. Lower crustal seismic velocity-anomalies; magmatic underplating or serpentinized peridotite? Evidence from the Vøring Margin, NE Atlantic. *Marine Geophysical Researches*, **23**, 169–183, https://doi.org/10.1023/a:1022480304527

Mjelde, R., Iwasaki, T., Shimamura, H., Kanazawa, T., Kodaira, S., Raum, T. & Hajime, S. 2003. Spatial relationship between recent compressional structures and older high-velocity crustal structures; examples from the Vøring Margin, NE Atlantic, and Northern Honshu, Japan. *Journal of Geodynamics*, **36**, 537–562, https://doi.org/10.1016/S0264-3707(03)00087-5

Mjelde, R., Raum, T., Breivik, A.J., Shimamura, H., Murai, Y., Takanami, T. & Faleide, J.I. 2005. Crustal structure of the Vøring Margin, NE Atlantic: a review of geological implications based on recent OBS data. *In*: Doré, A.G. & Vining, B.A. (eds) *Petroleum Geology: North-West Europe and Global Perspectives – Proceedings of the 6th Petroleum Geology Conference*. Geological Society, London, 803–813, https://doi.org/10.1144/0060803

Mjelde, R., Faleide, J.I., Breivik, A.J. & Raum, T. 2009*a*. Lower crustal composition and crustal lineaments on the Vøring Margin, NE Atlantic: a review. *Tectonophysics*, **472**, 183–193, https://doi.org/10.1016/j.tecto.2008.04.018

Mjelde, R., Raum, T., Kandilarov, A., Murai, Y. & Takanami, T. 2009*b*. Crustal structure and evolution of the outer Møre margin, NE Atlantic. *Tectonophysics*, **468**, 224–243, https://doi.org/10.1016/j.tecto.2008.06.003

Moore, D.E., Lockner, D.A., Ma, S. & Summers, R. 1997. Strengths of serpentinite gouges at elevated temperatures. *Journal of Geophysical Research*, **102**, 14,787–14,801, https://doi.org/10.1029/97JB00995

Morewood, N.C., Shannon, P.M. & Mackenzie, G.D. 2004. Seismic stratigraphy of the southern Rockall Basin: a comparison between wide-angle seismic and normal incidence reflection data. *Marine and Petroleum Geology*, **21**, 1149–1163, https://doi.org/10.1016/j.marpetgeo.2004.07.006

Morewood, N.C., Mackenzie, G.D., Shannon, P.M., O'Reilly, B.M., Readman, P.W. & Makris, J. 2005. The crustal structure and regional development of the Irish Atlantic margin region. *In*: Doré, A.G. & Vining, B.A. (eds) *Petroleum Geology: North-West Europe and Global Perspectives – Proceedings of the 6th Petroleum Geology Conference*. Geological Society, London, 1023–1033, https://doi.org/10.1144/0061023

Naylor, D., Shannon, P.M. & Murphy, N. 1999. *Irish Rockall Basin Region – A Standard Structural Nomenclature System*. Petroleum Affairs Division, Dublin, Special Publications, **1/99**.

Naylor, D., Shannon, P. & Murphy, N. 2002. *Porcupine-Goban Region – A Standard Structural Nomenclature System*. Petroleum Affairs Division, Dublin, Special Publications, **1/02**.

Nirrengarten, M., Gernigon, R.S. & Manatschal, G. 2014. Lower crustal bodies in the Møre volcanic rifted margin: Geophysical determination and geological implications. *Tectonophysics*, **636**, 143–157, https://doi.org/10.1016/j.tecto.2014.08.004

Olafsson, I., Sundvor, E., Eldholm, O. & Grue, K. 1992. Møre margin: crustal structure from analysis of expanded spread profiles. *Marine Geophysical Researches*, **14**, 137–163, https://doi.org/10.1007/BF01204284

O'Reilly, B.M., Hauser, F., Jacob, A.W.B. & Shannon, P.M. 1996. The lithosphere below the Rockall Trough: wide-angle seismic evidence for extensive serpentinisation. *Tectonophysics*, **255**, 1–23, https://doi.org/10.1016/0040-1951(95)00149-2

O'Reilly, B.M., Hauser, F., Ravaut, C., Shannon, P.M. & Readman, P.W. 2006. Crustal thinning, mantle exhumation and serpentinization in the Porcupine Basin, offshore Ireland: evidence from wide-angle seismic data. *Journal of the Geological Society, London*, **163**, 775–787, https://doi.org/10.1144/0016-76492005-079

Pascal, C. & Cloetingh, S.A.P.L. 2009. Gravitational potential stresses and stress field of passive continental margins: insights from the south-Norway shelf. *Earth and Planetary Science Letters*, **277**, 464–473, https://doi.org/10.1016/j.epsl.2008.11.014

Pauselli, C., Ranalli, G. & Federico, C. 2010. Rheology of the Northern Apennines: lateral variations of lithospheric strength. *Tectonophysics*, **484**, 27–35, https://doi.org/10.1016/j.tecto.2009.08.029

Pérez-Gussinyé, M. & Reston, T.J. 2001. Rheological evolution during extension at nonvolcanic rifted margins: onset of serpentinization and development of detachments leading to continental breakup. *Journal of Geophysical Research*, **106**, 3961–3975, https://doi.org/10.1029/2000jb900325

Péron-Pinvidic, G., Manatschal, G., Dean, S.M. & Minshull, T.A. 2008. Compressional structures on the West Iberia rifted margin: controls on their distribution. *In*: Johnson, H., Doré, A.G., Gatliff, R.W., Holdsworth, R., Lundin, E.R. & Ritchie, J.D. (eds) *The Nature and Origin of Compression in Passive Margins*. Geological Society, London, Special Publications, **306**, 169–183, https://doi.org/10.1144/sp306.8

Peron-Pinvidic, G., Manatschal, G. & Osmundsen, P.T. 2013. Structural comparison of archetypal Atlantic rifted margins: a review of observations and concepts. *Marine and Petroleum Geology*, **43**, 21–47, https://doi.org/10.1016/j.marpetgeo.2013.02.002

Petersen, U.K. & Funck, T. In press. Review of seismic refraction modelling in the Faroe–Shetland channel. *In*: Péron-Pinvidic, G., Hopper, J.R., Stoker, M.S., Gaina, C., Doornenbal, J.C., Funck, T. & Árting, U.E. (eds) *The NE Atlantic Region: A Reappraisal of Crustal Structure, Tectonostratigraphy and Magmatic Evolution*. Geological Society, London, Special Publications, **447**, https://doi.org/10.1144/SP447.7

Praeg, D., Stoker, M.S., Shannon, P.M., Ceramicola, S., Hjelstuen, B., Laberg, J.S. & Mathiesen, A. 2005. Episodic Cenozoic tectonism and the development of the NW European 'passive' continental margin. *Marine and Petroleum Geology*, **22**, 1007–1030, https://doi.org/10.1016/j.marpetgeo.2005.03.014

Raleigh, C.B. & Paterson, M.S. 1965. Experimental deformation of serpentinite and its tectonic implications. *Journal of Geophysical Research*, **70**, 3965–3985, https://doi.org/10.1029/JZ070i016p03965

Raum, T., Mjelde, R. *et al*. 2005. Sub-basalt structures east of the Faroe Islands revealed from wide-angle seismic and gravity data. *Petroleum Geoscience*, **11**, 291–308, https://doi.org/10.1144/1354-079304-627

Redfield, T.F. & Osmundsen, P.T. 2013. The long-term topographic response of a continent adjacent to a hyperextended margin: a case study from Scandinavia. *Geological Society of America Bulletin*, **125**, 184–200, https://doi.org/10.1130/B30691.1

Redfield, T.F. & Osmundsen, P.T. 2014. Some remarks on the earthquakes of Fennoscandia: a conceptual seismological model drawn from the perspective of hyperextension. *Norwegian Journal of Geology*, **94**, 233–262, https://doi.org/10.17850/njg94-4-01

Reinen, L.A., Weeks, J.D. & Tullis, T.E. 1994. Frictional behavior of lizardite and antigorite serpentinites: experiments, constitutive models, and implications for natural faults. *Pure and Applied Geophysics*, **143**, 317–358, https://doi.org/10.1007/BF00874334

Reynisson, R.F., Ebbing, J., Lundin, E., Osmundsen, P.T.A. & Usov, S. 2010. Properties and distribution of lower crustal bodies on the mid-Norwegian margin. *In*: Vining, B. & Pickering, S. (eds) *Petroleum Geology – From Mature Basins to New Frontiers. Proceedings of the 7th Petroleum Geology Conference*. Geological Society, London, UK, 843–854, https://doi.org/10.1144/0070843

Ritchie, J.D., Johnson, H. & Kimbell, G.S. 2003. The nature and age of Cenozoic contractional deformation within the NE Faroe–Shetland Basin. *Marine and Petroleum Geology*, **20**, 399–409, https://doi.org/10.1016/s0264-8172(03)00075-8

Ritchie, J.D., Johnson, H., Quinn, M.F. & Gatliff, R.W. 2008. Cenozoic compressional deformation within the Faroe–Shetland Basin and adjacent areas. *In*: Johnson, H., Doré, A.G., Gatliff, R.W., Holdsworth, R., Lundin, E.R. & Ritchie, J.D. (eds) *The Nature and Origin of Compression in Passive Margins*. Geological Society, London, Special Publications, **306**, 121–136, https://doi.org/10.1144/SP306.5

Ritchie, J.D., Ziska, H., Kimbell, G.S., Quinn, M. & Chadwick, A. 2011. Structure. *In*: Ritchie, J.D.,

Ziska, H., Johnson, H. & Evans, D. (eds) *The Geology of the Faroe–Shetland Basin, and Adjacent Areas*. British Geological Survey Research Report, RR/11/01, Jarðfeingi Research Report, RR/11/01. British Geological Survey, Nottingham, 9–70.

Ritchie, J.D., Johnson, H., Kimbell, G.S. & Quinn, M. 2013. Structure. *In*: Hitchen, K., Johnson, H. & Gatliff, R.W. (eds) *The Geology of the Rockall Basin and Adjacent Areas*. British Geological Survey Research Report, RR/12/03. British Geological Survey, Nottingham, 10–46.

Ritter, U., Zielinski, G.W., Weiss, H.M., Zielinski, R.L.B. & Saettem, J. 2004. Heat flow in the Voring Basin, Mid-Norwegian Shelf. *Petroleum Geoscience*, **10**, 353–365, https://doi.org/10.1144/1354-079303-616

Roberts, A.W., White, R.S. & Christie, P.A.F. 2009. Imaging igneous rocks on the North Atlantic rifted continental margin. *Geophysical Journal International*, **179**, 1024–1038, https://doi.org/10.1111/j.1365-246X.2009.04306.x

Rohrman, M. 2007. Prospectivity of volcanic basins: trap delineation and acreage de-risking. *American Association of Petroleum Geologists Bulletin*, **91**, 915–939, https://doi.org/10.1306/12150606017

Rüpke, L.H., Schmid, D.W., Perez-Gussinye, M. & Hartz, E. 2013. Interrelation between rifting, faulting, sedimentation, and mantle serpentinization during continental margin formation – including examples from the Norwegian Sea. *Geochemistry, Geophysics, Geosystems*, **14**, 4351–4369, https://doi.org/10.1002/ggge.20268

Schwartz, S., Guillot, S. *et al.* 2013. Pressure-temperature estimates of the lizardite/antigorite transition in high pressure serpentinites. *Lithos*, **178**, 197–210, https://doi.org/10.1016/j.lithos.2012.11.023

Shannon, P.M., Jacob, A.W.B., O'Reilly, B., Hauser, F., Readman, P.W. & Makris, J. 1999. Structural setting, geological development and basin modelling in the Rockall Trough. *In*: Fleet, A.J. & Boldy, S.A.R. (eds) *Petroleum Geology of Northwest Europe: Proceedings of the 5th Conference*. Geological Society, London, 421–431, https://doi.org/10.1144/0050421

Sibson, R.H. 1995. Selective fault reactivation during basin inversion: potential for fluid redistribution through fault-valve action. *In*: Buchanan, J.G. & Buchanan, P.G. (eds) *Basin Inversion*. Geological Society, London, Special Publications, **88**, 3–19, https://doi.org/10.1144/gsl.sp.1995.088.01.02

Skogseid, J., Pedersen, T., Eldholm, O. & Larsen, B.T. 1992. Tectonism and magmatism during NE Atlantic continental break-up: the Vøring Margin. *In*: Storey, B.C., Alabaster, T. & Pankhurst, R.J. (eds) *Magmatism and the Causes of Continental Break-up*. Geological Society, London, Special Publications, **68**, 305–320, https://doi.org/10.1144/gsl.sp.1992.068.01.19

Skogseid, J., Planke, S., Faleide, J.I., Pedersen, T., Eldholm, O. & Neverdal, F. 2000. NE Atlantic continental rifting and volcanic margin formation. *In*: Nøttvedt, A. (ed.) *Dynamics of the Norwegian Margin*. Geological Society, London, Special Publications, **167**, 295–326, https://doi.org/10.1144/GSL.SP.2000.167.01.12

Smallwood, J.R. & Kirk, W.J. 2005. Paleocene exploration in the Faroe–Shetland Channel: disappointments and discoveries. *In*: Doré, A.G. & Vining, B.A. (eds) *Petroleum Geology: North-West Europe and Global Perspectives – Proceedings of the 6th Petroleum Geology Conference*. Geological Society, London, 977–997, https://doi.org/10.1144/0060977

Stoker, M.S., Hoult, R.J. *et al.* 2005*a*. Sedimentary and oceanographic responses to early Neogene compression on the NW European margin. *Marine and Petroleum Geology*, **22**, 1031–1044, https://doi.org/10.1016/j.marpetgeo.2005.01.009

Stoker, M.S., Praeg, D. *et al.* 2005*b*. Neogene evolution of the Atlantic continental margin of NW Europe (Lofoten Islands to SE Ireland): anything but passive. *In*: Doré, A.G. & Vining, B.A. (eds) *Petroleum Geology: North-West Europe and Global Perspectives – Proceedings of the 6th Petroleum Geology Conference*. Geological Society, London, 1057–1076, https://doi.org/10.1144/0061057

Stoker, M.S., Leslie, A.B. & Smith, K. 2013. A record of Eocene (Stronsay Group) sedimentation in BGS borehole 99/3, offshore NW Britain: implications for early post-rift development of the Faroe–Shetland Basin. *Scottish Journal of Geology*, **49**, 133–148.

Stoker, M.S., Doornenbal, H., Hopper, J.R. & Gaina, C. 2014. Tectonostratigraphy. *In*: Hopper, J.R., Funck, T., Stoker, M., Arting, U., Peron-Pinvidic, G., Doornenbal, H. & Gaina, C. (eds) *NAG-TEC Atlas: Tectonostratigraphic Atlas of the North-East Atlantic Region*. Geological Survey of Denmark and Greenland (GEUS), Copenhagen, 129–212.

Sundvor, E., Eldholm, O., Gladczenko, T.P. & Planke, S. 2000. Norwegian–Greenland Sea thermal field. *In*: Nøttvedt, A. (ed.) *Dynamics of the Norwegian Margin*. Geological Society, London, Special Publications, **167**, 397–410, https://doi.org/10.1144/GSL.SP.2000.167.01.15

Tuitt, A., Underhill, J.R., Ritchie, J.D., Johnson, H. & Hitchen, K. 2010. Timing, controls and consequences of compression in the Rockall–Faroe area of the NE Atlantic margin. *In*: Vining, B. & Pickering, S. (eds) *Petroleum Geology: From Mature Basins to New Frontiers. Proceedings of the 7th Petroleum Geology Conference*. Geological Society, London, 963–977, https://doi.org/10.1144/0070963

Tullis, T.E., Horowitz, F.G. & Tullis, J. 1991. Flow laws of polyphase aggregates from end-member flow laws. *Journal of Geophysical Research*, **96**, 8081–8096, https://doi.org/10.1029/90JB02491

Turcotte, D.L. & Schubert, G. 2002. *Geodynamics*. 2nd edn. Cambridge University Press, Cambridge.

Turner, J.P. & Williams, G.A. 2004. Sedimentary basin inversion and intra-plate shortening. *Earth-Science Reviews*, **65**, 277–304, https://doi.org/10.1016/j.earscirev.2003.10.002

Unternehr, P., Péron-Pinvidic, G., Manatschal, G. & Sutra, E. 2010. Hyper-extended crust in the South Atlantic: in search of a model. *Petroleum Geoscience*, **16**, 207–215, https://doi.org/10.1144/1354-079309-904

VÅGNES, E., GABRIELSEN, R.H. & HAREMO, P. 1998. Late Cretaceous–Cenozoic intraplate contractional deformation at the Norwegian continental shelf: timing, magnitude and regional implications. *Tectonophysics*, **300**, 29–46, https://doi.org/10.1016/S0040-1951(98)00232-7

VAN WEES, J.D. & BEEKMAN, F. 2000. Lithosphere rheology during intraplate basin extension and inversion. *Tectonophysics*, **320**, 219–242, https://doi.org/10.1016/S0040-1951(00)00039-1

VOGT, U., MAKRIS, J., O'REILLY, B.M., HAUSER, F., READMAN, P.W., JACOB, A.W.B. & SHANNON, P.M. 1998. The Hatton Basin and continental margin: crustal structure from wide-angle seismic and gravity data. *Journal of Geophysical Research*, **103**, 12,545–12,566, https://doi.org/10.1029/98jb00604

WELFORD, J.K., SHANNON, P.M., O'REILLY, B.M. & HALL, J. 2012. Comparison of lithosphere structure across the Orphan Basin–Flemish Cap and Irish Atlantic conjugate continental margins from constrained 3D gravity inversions. *Journal of the Geological Society, London*, **169**, 405–420, https://doi.org/10.1144/0016-76492011-114

WHITE, R.S. & SMITH, L.K. 2009. Crustal structure of the Hatton and the conjugate east Greenland rifted volcanic continental margins, NE Atlantic. *Journal of Geophysical Research: Solid Earth*, **114**, B02305, https://doi.org/10.1144/0016-76492011-114

WHITE, R.S., SMITH, L.K., ROBERTS, A.W., CHRISTIE, P.A.F., KUSZNIR, N.J. & TEAM, I. 2008. Lower-crustal intrusion on the North Atlantic continental margin. *Nature*, **452**, 460–464, https://doi.org/10.1038/nature06687

WILKS, K.R. & CARTER, N.L. 1990. Rheology of some continental lower crustal rocks. *Tectonophysics*, **182**, 57–77, https://doi.org/10.1016/0040-1951(90)90342-6

XU, Y., SHANKLAND, T.J., LINHARDT, S., RUBIE, D.C., LANGENHORST, F. & KLASINSKI, K. 2004. Thermal diffusivity and conductivity of olivine, wadsleyite and ringwoodite to 20 GPa and 1373 K. *Physics of the Earth and Planetary Interiors*, **143**, 321–336, https://doi.org/10.1016/j.pepi.2004.03.005

ZANG, S.X., WEI, R.Q. & NING, J.Y. 2007. Effect of brittle fracture on the rheological structure of the lithosphere and its application in the Ordos. *Tectonophysics*, **429**, 267–285, https://doi.org/10.1016/j.tecto.2006.10.006

ZISKA, H. & VARMING, T. 2008. Palaeogene evolution of the Ymir and Wvyille Thomson ridges, European North Atlantic Margin. *In*: JOHNSON, H., DORÉ, A.G., GATLIFF, R.W., HOLDSWORTH, R., LUNDIN, E.R. & RITCHIE, J.D. (eds) *The Nature and Origin of Compression in Passive Margins*. Geological Society, London, Special Publications, **306**, 153–168, https://doi.org/10.1144/SP306.7